DUPLICATE

Forecasting Research

Forecasting Research Division
Technical Report No. 179

Impact of 3rd Climate Version Physics Changes on the Global Unified Model used for NWP

by

S F Milton and S J Lorrimer

December 1995

Meteorological Office
London Road
Bracknell
Berkshire
RG12 2SZ
United Kingdom

ORGS UKMO F
National Meteorological Library
FitzRoy Road, Exeter, Devon. EX1 3PB

Forecasting Research
Technical Report No. 179

Impact of 3rd Climate Version Physics Changes on the Global Unified Model used for NWP

by

S F Milton and S J Lorrimer

December 1995

Forecasting Research
Meteorological Office
London Road
Bracknell
Berkshire
RG12 2SZ
United Kingdom

© Crown Copyright 1995

This paper has not been peer-reviewed and should be regarded as an Internal Report from the Meteorological Office. Permission to quote from it should be obtained from the above Meteorological Office division.

IMPACT OF 3RD CLIMATE VERSION PHYSICS CHANGES ON THE GLOBAL UNIFIED MODEL USED FOR NWP.

S.F. Milton and S.J. Lorrimer.

1. INTRODUCTION

This paper discusses the impact of the 3rd climate version (3CV) physics package upon the performance of the global Unified Model as used for operational NWP. The performance is assessed largely on the impact the changes have on the large scale circulation and in particular the systematic errors of the model. A comprehensive review of the systematic errors in the current and previous operational versions can be found in Milton et al. (1995a). An additional set of sensitivity tests are also discussed which relate to a correction in the boundary layer code and improvements to turbulent mixing of momentum.

2. SCIENTIFIC DETAILS OF CHANGES TESTED

A full list of the changes implemented in the climate model can be found in Appendix A. Only a subset of these were tested in the operational UM as a number are already operational or have been tested. The acronyms in brackets shall be used in the remainder of the text when discussing the impacts.

a) Improvements to the formulation of mixed phase clouds. (FOCWWIL)
In the Operational Global Model mixed phase cloud exists in the temperature range $-15 < T-T_m < 0$, where T is temperature and T_m the melting point of ice. The fraction of ice and water between these temperatures is given by a quadratic spline.

Recent work at MRF (Moss and Johnson, 1995) has suggested that a parametrization for mixed clouds with a linear fit between 264K and 273K is more in accord with observations. This has been coded for the UM with a linear fit in the regime $-9 < T-T_m < 0$.

b) Correction to saturation vapour pressure (QSAT)
In the current formulation of the UM the saturated specific humidity is given by (Smith, Gregory and Wilson, UM Doc Paper 29)

$$q_s(T,p) = \frac{\epsilon e_s(T)}{p} \qquad (1)$$

Where e_s is the saturation vapour pressure of water vapour and ε is the ratio of the molecular weights of water and dry air. This equation is an approximation of the more accurate relation,

$$q_s(T,p) = \frac{\epsilon e_s(T)}{(p - (1 - \epsilon)e_s(T))} \qquad (2)$$

A modification is made to use this more accurate equation. In addition e_s is defined in UM Doc. Paper 29 as the saturation vapour pressure of water vapour in the pure phase (i.e over a plane water surface). However a correction needs to be applied to obtain the saturation vapour pressure for *moist air*, and this modification is also made. The result is that the saturated specific humidites are higher for a given temperatures. Further discussion of the saturated specific humidity can be found in Gill (1982).

c) MRF/UMIST parametrization for effective radius of water drops (RE)
This modification amends the the parametrization of cloud microphysics so that the effective radius of liquid water droplets, the ratio of the volume mean radius to the effective radius and the concentration of activated cloud condensation nuclei are all functions of whether the point is maritime or continental. This is based on work by MRF.

d) Modifications to Large Scale Precipitation and improvements to the evaporation of precipitation (Large scale + Convective) (LPPN)
The large scale precipitation parametrization in the UM (Smith, Gregory and Mitchell, 1993;UMDP 26) is based on a scheme developed for cloud scale models. It has been pointed out that in these 'cloud-scale' schemes the parametrization of autoconversion (growth of raindrops from cloud drops) is based upon the assumption that cloud properties are uniform in the gridbox. Clearly for the large gridscales of the operational (~100km) and climate (~250km) versions of the UM this is not a valid assumption. In order to account for non-uniform cloud properties the precipitation rates are now determined accounting for the distribution of cloud water contents within the cloudy part of the grid box as implied by the distribution of total water used in layer cloud scheme. The distribution statistics (Q_c and b_s - see UMDP 29) are passed from the large scale cloud scheme to the large scale precipiation scheme and are used to recreate a moisture distribution consistent with the cloud field. This allows non-zero precipitation rates to exist for subsaturated gridboxes.

A modified treatment of ice precipitation has been formulated, which involves changes to the ice fallout calculation to improve long time-step behaviour. Two modifications to the ice fallout scheme are made. For timesteps less than the time for infalling ice to cross the layer, the flux divergence scheme is retained, but with explicit formulation. For long timestep the final ice content equilibrates to the incoming ice flux and the mean outgoing ice flux is adjusted consistently. It should be noted that in the current operational model the ice precipitation falls to the ground in 1 timestep as allowing ice precipitation to contribute to cloud water in lower layers only increases the occurrence of unrealistic superadiabatic profiles in the forecasts (Wilson et. al., 1994).

A corrected treatment of the evaporation of rain and snow for both large scale and convective precipitation is made, mainly including a pressure dependency.

e) FULL 3CV

This is the full package of changes (a) to (d). Note: This is not the full package as run in climate simulations, which is given at Appendix A.

3. DETAILS OF CASE STUDIES.

A set of 5 case study forecasts for both winter (January-February) and summer (June-August) were run for each of the 3CV changes from the UKMO operational 00Z analyses on the dates shown below.

Winter	Summer
15.01.95	01.06.94
26.01.95	23.06.94
06.07.95	15.07.94
17.02.95	06.08.94
28.02.95	28.08.94

Each forecast is run to 5 days and most of the results discussed are for the 5 case means of winter and summer forecasts. All Model validation and verification is carried out against the UKMO operational analyses. Verification against observations will be carried out in the parallel trial of 3CV physics.

4. CONTROL INTEGRATIONS.

In order to assess the impacts of 3CV we present here the zonally averaged mean errors (Forecast - Analysis) of the control integrations at T+120 and discuss how representative the errors over this small sample are of the systematic errors in a larger sample of operational forecasts (see Milton et al (1995a)).

Figure 1 shows the mean errors in the zonally averaged zonal wind. General features are westerly errors in midlatitudes at 60N and 60S and also in the tropic/subtropics at 20N-30N and 20S and easterly errors elsewhere. In the extratropics the errors maintain the same sign with height (barotropic) whereas in the tropics in Jan/Feb 95 we have easterly errors in the boundary layer westerly errors in mid troposphere and easterly errors in the stratosphere. The structure of these errors is very similar to those shown in Milton et. al. (1995a) averaged over one month of forecasts.

In both Jan/Feb and Jun/Aug the Hadley cell in the model is too intense in the upper tropical troposphere (Fig. 2). This is thought to be partly due to excessive parametrized diabatic heating in the tropics.

The zonally averaged mean errors for temperature (Fig. 3) show the familiar cold bias in the extratropics and at the tropopause of order 1K at T+120. In the tropical mid troposphere we have a warming of ~0.4K, with similar warmings in the stratosphere at ~100mb.

5. IMPACT OF 3CV CHANGES ON MODEL CLIMATE.

a) Cloud and moisture variables

We begin with changes to the cloud and moisture fields as these changes have the biggest impact on the model's temperature fields and top of the atmosphere (TOA) radiation balance.

Figure 4(a) shows the zonally averaged layer cloud distribution for the Jan/Feb 95 cases. FOCWWIL reduces the layer cloud fraction by 2% in the northern hemisphere extratropics (cloud fraction change, not percentage change) and by 4% in the southern hemisphere (Fig 4(b)). The FOCWWIL change increases the proportion of cloud ice to cloud water at a given temperature in the range $-9<T-T_m<0$, and as the residence time for the ice phase is less than that for the water phase then cloud amounts are reduced.

QSAT leads to a very small increase in layer cloud at the tropical tropopause where convection detrains (Fig. 4(c)). The increases are due to the water content of convective parcels being increased .

RE very slightly reduces the cloud at 30S as a consequence of a warming due to the change in the SW properties of the cloud (Fig. 4(d)).

The biggest impact on layer cloud comes from the LPPN changes (Fig. 4(e)). Over the poles we see an increase in low level cloud fractions of ~20%. This can be explained by the fact that the control integrations allow ice precipitation to fall to the ground in 1 timestep whereas in the LPPN runs the ice precipitation is allowed fall into lower layers and increase cloud ice. Elsewhere we see reductions in layer cloud due to LPPN, particularly at the tropopause. This may be due precipitation formation being allowed for subsaturated gridboxes.

For Full 3CV (Fig. 4(f)) the cloud increases in the boundary layer over the poles and tropical tropopause and reduces elsewhere. The largest reductions of ~4% between 30S and 60S are thought to be particularly beneficial as excessive low cloud in the southern hemisphere storm track may be responsible for the large cold bias in the control runs at this location (see discussion in Milton et al., 1995a).

Figure 4B shows the changes in the moist variables at T+120 for Jan/Feb 95 due to Full 3CV. The specific humidity increases by 1% in the tropical lower troposphere due to the increased saturation specific humidity arising from the QSAT change (Fig. 4B(b)). Cloud liquid water is decreased almost everywhere by ~10% due to both FOCWWIL and LPPN (Fig. 4B(d)). Cloud ice increases over the poles by 50%-100% due to changes to ice fallout in LPPN and elewhere is reduced.

For convective cloud (Fig. 5(a)) QSAT has the biggest impact increasing cloud fractions by 0.4% (Fig. 5(c)) throughout the depth of the tropical troposphere. LPPN (Fig. 5(e)) shows increased cloud in the upper tropical troposphere and at 60S and reductions at 40S. FOCWWIL also reduces convective cloud amount in the southern hemisphere. This must be due to an indirect feedback with the convection scheme. For the Jun/Aug 94 cases we see similar signals in both layer and convective cloud (Fig. 6). The reductions in layer cloud over

the northern hemisphere pole are particularly marked.

The reductions in cloud amount can be clearly seen in the latitudinal profiles of total cloud amount (max/random overlap) shown in Figure 7. The exception is over the poles in Jan/Feb 95 where total cloud increases. Figure 8 shows the differences in total cloud amount (3CV-Control) for land and oceans separately. Reductions in cloud cover of 5%-10% occur over *both* land and ocean.

b) Zonally Averaged Temperatures and Diabatic heating.

Figure 9(a) shows the zonal mean temperature for T+96 to T+120 (Degrees Celsius); the vertical coordinate is model level and the right hand axis shows approximate pressure. The impact of 3CV is a general warming of up to 0.2K, although 0.05K is more typical (Fig. 9(f)). There are some small areas of cooling, especially near the poles. Figures 9(b)-(e) show the impact of each element of the package. The warming in the tropics is due to heating by QSAT (Fig. 9(c)) which is partially compensated for by cooling in LPPN (Figure 9(e)). In high latitudes, where the impact of QSAT is much reduced, LPPN dominates, and so temperatures near the poles are reduced, especially near the surface. FOCWWIL warms the extratropics by ~0.1 K (Fig. 9(b)), and counteracts the effect of LPPN at high latitudes. There is a maximum in its warming at 60S, model level 5 (see also Fig. 9(f)). RE (Fig. 9(d)) is only of significance in the southern hemisphere extra-tropics, where there is a warming of up to 0.075K. The warming maxima of both FOCWWIL and RE are reinforced by LPPN in this region. In the upper stratosphere there is a cooling of up to 0.05K in full 3CV, due to RE, FOCWWIL and QSAT. The net response to 3CV is very similar for the Jun/Aug 94 cases (Fig. 10). We now discuss the winter cases in more detail.

Comparing the impact of 3CV (Figure 9(f)) with the mean errors in the control (Figure 3(b)), we see that the general warming is beneficial, especially in the southern hemisphere stormtrack. Also Figure 9(f) shows a large additional cooling near the surface in the Northern Hemisphere. This coincides with a warm error in Figure 3(b), although in systematic errors from a larger number of cases a systematic cooling of the surface is more usual (Milton et al., 1995a). More worrying is the peak in warming in Figure 9(f) in the tropics at 400mb as this coincides with a warming error in Figure 3(b). Similarly, in mid and high latitudes around 400mb the 3CV package leads to an additional cooling, which coincides with an existing cold error. The impact of 3CV on temperatures is relatively small (~10%), being of the order 0.05K to 0.1K at T+120 compared to typical errors of 0.5K to 1.0K.

Figure 11 shows the radiative heating tendencies averaged between T+00 and T+24. The panels are equivalent to those in Figure 9. Comparing Figures 11(e) and 11(f), LPPN causes much of the change in radiative heating seen in Full 3CV. LPPN increases cloud near the tropical tropopause (level 12) with a reduction in cloud just above it (Fig 4(e)). This leads to an increase in cloud top cooling, peaking at level 12-13 in the tropics. In the extratropics cloud decreases at the tropopause and this leads to cooling in the layers below due a decrease in downward longwave radiation, and a slight warming in upper layers where cloud top cooling has been reduced. In the mid-latitude boundary layer, LPPN leads to an increase in cloud. This causes an increase in cloud top cooling (level 4) and base heating(level 1) (Slingo & Slingo 1988). FOCWWIL leads to reductions in cloud amount (Figure 4(b)). Therefore,

there are reductions in cloud top cooling and, to a lesser extent, base heating. Most of the changes in radiative heating are associated with changes in cloud, except RE which *directly* affects the short wave heating in grid boxes containing water-cloud.

The net effect of 3CV on convection is a cooling near the surface and mid troposphere in the tropics(Figure 12(f)). The top of the convective column warms in the tropics. The largest contribution is from QSAT (Figure 12(c)). The pattern of changes suggests there is a general increase in convective activity. There is some evidence that the cooling in the lower layers is less evident at later time ranges when the warming dominates. QSAT increases the saturation specific humidity and so allows the air to be slightly moister for a given temperature (see Fig 4B(b)). Therefore, during convection a parcel will be moister and ascend a warmer moist adiabat. Although the change in saturation humidity is small, the moist adiabats diverge rapidly as altitude increases leading to a marked additional latent heat release in the upper troposphere compared to the control runs. The changes in convective heating due to LPPN are more complex (Figure 12(e)). In the tropics there is a reduction in convective activity in the lower troposphere but an increase in the upper troposphere. There is also a response in the extratropics. These changes in convective heating must be associated with changes in stability, for example LPPN cools the upper layers making them more unstable and hence increasing convection.

Figure 13 shows the impact on boundary layer heating by turbulent mixing. The contour interval in Figures 13(b)-(f) is 0.1K day^{-1}. In the Northern Hemisphere LPPN (Figure 13(e)) shows a large additional heating in model levels 1-3, with a cooling in level 4. The same is true in the Southern Hemisphere, but to a lesser extent. The cooling produced by LPPN near to the surface (mainly by the evaporation of cloud - see Fig. 14(e) and 14B(b)) is probably leading to an increase in the turbulent heat flux, and so to the additional boundary layer warming. The reduction in boundary layer warming above this suggests that the turbulent mixing is not penetrating as far up into the atmosphere.

Figure 14 shows the impact of large-scale condensation. This includes evaporation of precipitation and both calls to the large-scale cloud scheme (one explicit call and one call within the boundary layer scheme). The contour interval is 0.1K day^{-1}. Most of the impact is due to LPPN (Figure 14(e)), which counteracts the changes turbulent mixing (Figure 13(e)). The changes to latent heating in level 4 are straightforward; LPPN leads to an increase in cloud amount and so an increased latent heat release. Below this however, is a very strong cooling in a region where large scale cloud amounts have increased!. This apparent paradox is explained by reference to Fig. 14B(b) which shows the temperature tendency due to the large-scale cloud alone (no evaporation of precipitation) when using 3CV. Despite the increase in large-scale cloud, there is a negative latent heat release in the lowest layers (*cf* the control, Figure 14B(a)). This suggests that the extra low cloud is being generated by the accumulation of precipitating ice. The flux divergent fallout scheme allows cloud ice from the layers above to form cloud directly in the lower layers. Subsequently, the large-scale cloud scheme dissipates some cloud, causing a negative latent heat release and a cooling in the overall large scale condensation increments (Fig. 14(f)).

The impact of the various components of 3CV on the net parametrized tendency (*ie* the

diabatic heating, Fig. 15) is for warming in mid troposphere and cooling in the lowest layers. The biggest impact is due to LPPN, although this is opposed in the tropics by QSAT. FOCCWIL has a small impact, warming in mid-latitudes. The impact of RE is small and highly localised.

Figure 16 shows the total tendency (dynamics + parametrizations). When averaged over sufficient cases this shows the model systematic error (Milton 1993). For example the total tendency in the control (Fig.16(a)) bears a strong resemblance to the systematic error at T+120 (Fig 3(b)). A useful measure of the impact of the changes on the systematic error of the model is therefore a comparison of Figures 16(a) and (f). Note that the contours intervals are very different; the contour interval in Figure 16(a) is around ten times that in Figure 16(f). Therefore, any impact on the model systematic error must be small. On the positive side, Figure 16(f) shows a warming around model level 6 in mid and high-latitudes. This helps to correct the existing error, particularly around 50S, where there is a persistent area of significant cold bias (*cf* Figure 16(a) and 3(b)). The improvement in this area is due to FOCWWIL and RE (Figures 16(b) and (d)). Negative aspects include; an additional cooling of 0.05K day^{-1} occurs near the tropopause where there is already a cooling tendency of up to 0.6K day^{-1} (Figure 16(a)); additional warming of 0.025 K day^{-1} at model level 10 in the tropics where there is already an erroneous tendency to warm in the control.

As one might expect the net impact on the *thermal tendency* between T+00 and T+24 (Fig. 14(f)) and the change in *temperature* meaned over T+96 to T+120 (Fig. 9(f)), are similar in many respects with warming in the lower and mid troposphere and surface cooling in the Northern hemisphere. However at the tropopause the impact on the *thermal tendency* is for additional cooling whilst the *temperature* response is for a beneficial warming. This can be explained by the fact that the warming tendency due to QSAT (largely convective - Fig 12(c)) increases with time and becomes dominant over the cooling tendency of LPPN (largely radiative - Fig. 11(d)) at later forecast ranges. This is explained by the fact that the analyses were created from the 'control' physics and it takes a finite time for the increase in tropical moisture (and hence convective heating) due to QSAT to spin up.

Overall, the thermal impact of the 3CV package is small, but by T+120 is mainly beneficial.

c) Zonally Averaged Winds.

The clearest impact in the winds apears to be in the meridional component (Fig. 17). In both Jan/Feb 95 and Jun/Aug 94 cases the impact of 3CV is to increase the Hadley circulation by ~3% (0.1 m/s) at T+120. As the Hadley circulation is already too intense in the control integrations by ~50% at T+120 (Fig. 2) this represents a small negative impact. The increased Hadley circulation is a direct response to the increased diabatic heating in the tropics in 3CV discussed in the previous section.

In the zonal wind we see that the impact of 3CV in the tropical/subtropical regions (30N-30S) is for increased westerlies at jet level (Fig. 18). This generally leads to increases in the mean errors in these regions. The impacts are small and only of order 0.2 m/s compared to typical mean errors of ~2m/s (Fig. 1).

The mean errors in the zonally averaged winds and temperature for Jan/Feb 95 Full 3CV runs (Fig. 19) show that overall the impacts lead to very little change in the magnitude of the existing errors in the control runs (Fig. 1 - 3).

d) Precipitation.

The main impact of 3CV on total precipitation is a 2-3% increase in the 5 day accumulations in the tropics (Figure 20(f) and 21(f)). Most of this comes from convective precipitation and is largely associated with the increased diabatic heating due to the QSAT change. Considering the *precipitation rates* at T+96 to T+120 we see slightly larger increases of ~5% in total precipitation rate. This is consistent with the spin-up in the changes due to QSAT discussed in section 5(b). It is believed that tropical precipitation in the UM may already be too high in the early forecast periods since the change to moisture assimilation made in November 1994 (Bell, 1994). This is supported by comparisons with the GOES precipitation index (Janowiak, 1992 - based on cloud top temperature), and the Legates and Willmott (1990) precipitation climatology. In addition tropical precipiation now spins down with forecast range between T+00 and T+72 (Milton et al., 1995a).

e) MSLP.

Changes in the large scale circulation are very small (Fig. 22). Mean errors in MSLP for the controls are typically ~5 to 10 mb at T+120 and in most regions the impact of 3CV is less than 1mb. Some differences of order 1mb can be seen in the N. Atlantic, but one cannot attach any great statistical significance to such small changes over such a small number of forecasts.

h) TOA radiative fluxes - Comparisons with ERBE

Given the general decreases in total cloud cover, we need to assess whether such decreases are beneficial . One way to indirectly validate global cloud cover is to study the top of the atmosphere (TOA) radiation budget. The remainder of this section compares model TOA radiative fluxes for T+96 to T+120 and contrasts them with ERBE measurements for January and August 1988. Although the model and ERBE measurements are from different years the the differences between the model and ERBE are much larger than any interannual variations in the ERBE measurements. To minimize interannual fluctuations we confine ourselves to looking at zonal averages.

The OLR in the model is consistently too large compared to ERBE (Fig 23 (a) and (b)) and the reductions in cloud amount in 3CV make this error marginally worse (see global mean values). However it should be noted that a large proportion of the error in OLR appears to be in the clear sky component (Fig. (c) and (d)). Examination of the geographical distributions (not shown) shows that the problem is located over land and may be a function of incorrect surface temperatures.

The 3CV changes lead to a reduction in the planetary albedo of the model (Fig. 24 (a) and (b)), which is generally an improvement as the planetary albedo in the control runs is too large. This is due to the reductions in cloud amount, particularly the low cloud.

Given that the clear sky albedo of the model is an underestimate at most latitudes (Fig. 24(c)

and (d)) and the planetary albedo an overestimate then the SW radiative forcing of clouds must show large errors. The SW cloud forcing (SWCF) is defined as

$$SWCF=S(\alpha_c-\alpha) \quad (3)$$

where S is the incoming solar flux, α_c is the clear sky albedo and α is the albedo for cloudy skies. SWCF is negative (Fig. 25) showing that clouds act to cool the atmosphere in the shortwave by reflecting incoming radiation. The SWCF in the model is overestimated (Fig.25) ,with particularly large errors in Jul/Aug 94 in the summer hemisphere. In general the reductions in cloud in 3CV lead to improvements in SWCF bringing the model closer to ERBE. An exception is over the southern oceans (60S) in Jan/Feb 95 where the differences between the model and ERBE appear to be dominated by an incorrect positioning of the cloud maxima at 40-50S compared to 60S suggested by the ERBE results.

The longwave cloud forcing (LWCF) is defined as

$$LWCF = OLR_c - OLR \quad (4)$$

LWCF is a positive quantity as clouds warm the atmosphere in the LW region due to the greenhouse effect. In Jan/Feb 95 the control integrations underestimate LWCF between 50N and the equator and tend to overerestimate it elsewhere (Fig. 25). Agreement between the model and ERBE is very good in Jul/Aug 94. The reductions in cloud in 3CV lead to reductions in LWCF which is beneficial at high latitudes but not in the tropics/subtropics. The globally averaged values suggest that the control integrations are closer to ERBE.

Finally we note that there is considerable spinup in the cloud forecasts. Figure 26 shows the SWCF and LWCF for T+00 to T+24 during Jun/Aug 94. The SWCF is clearly a much better fit to ERBE than at T+96 to T+120, and the 3CV forecasts are closer than the control. This may suggest that the low cloud fields in particular are more accurate earlier in the forecasts. Conversely the LWCF is a slightly worse fit to ERBE in the earlier forecast ranges and the 3CV is worse than the control. It should also be noted that the spinup in cloud has been reduced since changes to the moisture assimilation made in November 1994 (Bell,1994).

In summary the planetary albedos and SWCF in 3CV are closer to ERBE than the control runs as a consequence of reductions in cloud cover. The OLR and LWCF are made marginally worse in 3CV with respect to ERBE. Unfortunately we still do not know if the outstanding errors in the TOA radiative fluxes are largely due to incorrect cloud amounts, incorrect cloud radiative properties, or a combination of both.

i) Surface fluxes

Changes to the SW and LW surface radiative fluxes (positive downwards) are in line with reductions in cloud cover and compensate each other (Fig. 27). The net SW surface flux increases at all latitudes due to greater incoming solar radiation. The net LW surface flux becomes more negative implying a larger cooling of the earths surface. This is due a reduction

in the downwelling radiation from clouds. The turbulent fluxes (positive upwards) show little change. The sensible heat fluxes in 3CV and controls are virtually identical. The latent heat flux in 3CV is increased slightly.

j) Occurrence of superadiabatic profiles

With the re-introduction in 3CV of an ice fallout scheme allowing ice precipitation to contribute to cloud water in the lower layers we need to check that this does not increase the superadiabatic lapse rates in the model. One of the winter cases was rerun for both the control and 3CV formulations and a count of the occurrence of superadiabats showed no significant difference between Full 3CV and the control.

6. SENSITIVITY TESTS WITH BOUNDARY LAYER MIXING

A coding error was introduced into the boundary layer code when orographic roughness was introduced in January 1995. This error led to the boundary layer depth being overestimated by one model level. The Blackadar formula for mixing lengths is (Smith,UM Doc. Paper 24)

$$l_m(z) = \frac{k\,(z + z_{0m})}{1 + \dfrac{k\,(z + z_{0m})}{\lambda_m}} \qquad (5)$$

Where l_m is the mixing length, k von Karmans constant, z_{0m} the roughness length for momentum, and λ_m the assymptotic mixing length for momentum. This latter term is dependent on the boundary layer depth, z_h via the relation for the assymptotic mixing length $\lambda_m = \max(40.0, 0.15\, z_h)$. Thus an increase in z_h increases λ_m which leads to larger mixing lengths for momentum (l_m). This leads to enhanced turbulent mixing for momentum.

Unfortunately the increased mixing is actually beneficial to both the operational forecasts and climate simulations. Figure 28(b) shows the impact of correcting the error on the zonally averaged zonal wind at T+96 to T+120 . Westerly winds increase in mid-latitudes and easterlies in the tropics by 0.3 to 0.5 m/s. Consequently, correcting the error does marginally degrade the forecasts and removes some of the benefit gained from the original change to include orographic roughness and the new gravity wave drag scheme in January 1995 (Milton et al., 1995b) which were of the order 1.5 to 2.5 m/s. The changes to the boundary layer turbulent mixing during T+00 to T+24 are shown in Figure 29(b). The dipole pattern of negative below positive is indicative of a reduction in turbulent mixing of momentum.

Additional tests have been run which double the asymptotic mixing length for momentum (0.15 to 0.30) whilst also correcting the original error. This is an attempt to increase the turbulent mixing in a physically based way. The aim is to create a null change with respect to the current operational model (control) which contains the original error. Changes to the zonally averaged zonal wind are of the order 0.1 m/s at T+120 (Fig. 29(c)). Changes to the boundary layer turbulent mixing are small (~| 0.5 | m/s/day) compared to the impact of correcting the original error without doubling the mixing lengths (~ | 3.0 | m/s/day).

Figure 30 shows the impact of the changes in boundary layer turbulent mixing on the 850mb wind speed bias. In most areas (except the southern hemisphere) correcting the error in the boundary layer routine (BL Correction) makes the bias worse compared to the control, whilst the combination of the error correction and a doubling of the mixing lengths (AMIXLEN2) reduces biases again to levels very similar to those in the control.

On this evidence we recommend that the original error to the boundary layer be corrected and that the asymptotic mixing length is doubled to effectively give a null change with respect to the control forecasts.

7. OBJECTIVE VERIFICATION

(a) Calculation of scores

To make an objective assessment of the impact of the various modifications discussed above, we have verified the test and control forecasts against operational analyses. This is not ideal as the verification scores will be biased towards the model that generated the analyses. Thus, the objective verification will tend to favour the control forecasts. More significantly here, verification can only be carried out for five cases in each season. Much of the systematic change between forecasts will be lost in the noise due to the differences between cases. We therefore have to be particularly careful when comparing scores.

We have verified 15 different fields: 10m wind speed, 10m vector wind error, PMSL and temperature, geopotential height, wind speed and vector wind error at 250hPa, 500hPa and 850hPa. Each of these fields has been verified in five areas: globally, Northern Hemisphere above 30N, Tropics between 30N and 30S, Southern Hemisphere below 30S and area 2 (roughly the LAM area). Further, we verify each field at T+24, T+72 and T+120. We calculated the bias, RMS error and SD. We have therefore calculated 135 scores in each area for each test.

(b) 3CV

Table 1 (Appendix B) summarises the number of scores that improved, deteriorated or remained unchanged (where changes must be > 1%) when we used the full 3CV package for the five Jan/Feb 95 cases. The figures in brackets refer to the five Jun/Aug 94 cases. The vast majority of scores are unchanged. None of the RMS errors or SD's changed significantly. Considering each verification area separately, the only areas in which there are clear indications of any change are in the global scores for both seasons and in the Jun/Aug 94 Southern Hemisphere scores.

The global verification of the 3CV package shows a significant impact only in the temperature and height biases. Table 2 summarises the temperature and height biases for the control, and Table 3 summarises the biases for the 3CV package. There is a consistent improvement in biases at both T+72 and T+120 of around 10%. Breaking down the global temperature biases into the impact of different parts of the package (Fig 31), we can see that much of the improvement in temperature is due to QSAT, particularly at 250hPa and 500hPa. At 850hPa LPPN (not shown here) is probably also important. The impact of QSAT is even more significant in the tropics (Fig 32). Again the impact increases dramatically with height, but

it is notable at 500hPa, where the cold bias becomes a warm bias on implementing 3CV. Just above this, at 400hPa, there is a warm bias in the control (Fig 3(b)), which has been made worse by QSAT. The relatively large impact of 3CV in the tropics tends to dominate the global scores. The northern hemisphere scores (Fig 33) show that at 500hPa the cold bias increases slightly; again this is probably due to LPPN. At 250hPa and 850 hPa there is a small improvement at T+120.

The verification scores are consistent with the objective assessment, which showed a widespread, slight warming helping to correct cold biases (*cf* Figure 3(b) with 9(f), and 3(d) with 10(b)).

8. SUMMARY

In general most of the impact of 3CV is either small or neutral. The most coherent change is in the temperature field where we have a small beneficial warming. Below we summarise some of the positive and negative aspects of the Full 3CV package (not including changes to the boundary layer turbulent mixing).

Advantages of 3CV

- Warming
  - Tropopause
  - SH Stormtrack
- Reductions cloud
  - Tropopause
  - SH stormtrack
- Improved planetary albedo
- Improved SW cloud forcing

Disadvantages of 3CV

- Increased warming/diabatic heating in tropical mid troposphere
- Increased Hadley circulation.
- Increased tropical precipitation.
- Increased cloud in layer 1 at high latitudes.

REFERENCES

Bell, R.S. 1994: Revised moisture assimilation - results of a parallel trial. *FR Division Technical Report No. 132.*

Gill, A.E., 1982:'Atmosphere-Ocean Dynamics', Academic Press.

Janowiak, J.E., 1992: Tropical Rainfall: A comparison of satellite derived rainfall estimates with model precipitation forecasts, climatologies and observations. *Mon. Weath. Rev, 120, 448 - 462.*

Legates, D.R and C.J. Willmott, 1990: Mean and Seasonal spatial variability in gauge corrected global precipitation. *Int. J. of Climate, 10,111,127.*

Milton, S.F., 1993: Diagnosing systematic errors in the unified model I - Thermal budget. *FR Division Technical Report No. 64.*

Milton, S.F., C.A. Wilson and A. Van der Wal, 1995a: A review of systematic errors in the global Unified Model used for NWP 1994-95. FR Division Technical Report No. 162.

Milton, S.F., C.A. Wilson, O.M. Hammon and F. Rawlins, 1995b: Impact of a new gravity wave drag scheme and orographic roughness in the unified model. III Revised schemes and second parallel suite trial for global and limited area models. *FR Division Technical Report No. 139.*

Moss, S.J. and D.W. Johnson, 1994: Aircraft measurements to validate and improve numerical model parametrizations of ice to water ratios in cloud.*Atmos. Res, 34, 1-25.*

Slingo, A. and J.M. Slingo, 1988: The response of a general circulation model to cloud longwave radiative forcing. I - Introduction and initial experiments. *Quart. J.R. Meteorol.Soc., 114,1027-1062.*

Smith, R.N.B., 1993:Subsurface,Surface and Boundary Layer Processes. *UM Doc Paper No.24*

Smith, R.N.B., D.Gregory, J.F.B. Mitchell and A.C. Bushell 1995:Large Scale Precipitation. *UM Doc Paper No.26*

Wilson,C.A. , F. Rawlins and O.M. Hammon and , 1994: Cause and cure of the superadiabatic lapse rate in the limited area and global models. *FR Division Technical Report No. 125.*

APPENDIX A: 3RD CLIMATE VERSION CHANGES

Below is a full list of the changes for the 3rd climate version as implemented into the climate model. Those shown in bold are the ones which have been tested and are discussed in this paper. A number of changes have already been implemented operationally in both the globel model and LAM and are shown by OP.

a) Modification of temperature range of mixed phase clouds to match observations of MRF (tested in OP - S. Lorrimer)

b) Restriction of rapidly mixing term in BL scheme to below convective cloud base (Tested in OP - Rejected).

c) Local correction for negative specific humidity (Tested in OP parallel trial) - Rejected due to excessive cost.

d) Effective radius for water drops determined from MRF/UMIST parametrization using specified aerosol valuse with a land sea contrast.

e) Modified LS PPN scheme including

(i) Precip. rates are determined accounting for the distribution of cloud water contents within the cloudy part of the grid box as implied by the distribution of total water used in layer cloud scheme.(cf. Peter Jonas note 1993)

(ii) Modified treatment of ice precipitation - Changes the ice fallout calculation to improve long time-step behaviour.

f) Multi-layer soil hydrology - To be tested in Mesoscale model.

g) Revised GWD scheme (OP) - Coefficients at climate resolution have been changed at 3CV from values originally tested using 2CV (CLIM - TEST)

.

The current and past values for the gravity wave coefficients are shown below for the operational model (OPER/NWP) and for various climate configurations (CLIM)

	OPER/NWP 0.833 x 1.25	CLIM -TEST 2.5 x 3.75	CLIM - 3CV 2.5 x 3.75	CLIM-OPRES 0.833 x 1.25
KAY	1.0E+04	1.2E+04	2.0E+04	1.6E+04
KAY_LEE	1.8E+05	1.8E+05	3.0E+05	2.4E+04

h) Orographic roughness scheme. (OP)

i) Correction to specification of saturation humidity mixing ratio.

j) Corrected treatment of the evaporation of rain and snow (mainly including a pressure dependency).

k) No horizontal diffusion on steep surfaces - Operational since 20 June 1995.

l) Increased horizontal diffusion coefficients (u,v,theta, q - 12 hr e-folding time (compared with 24 Hr in 2CV) is used with del6 except for q above 150mb where an e-folding of 4 hrs and del4 is used)

m) Reformulation of surface exchange coeff. for scalars + 10m wind interpol. (OP - Included with Jan 95 O.Roughness changes)

APPENDIX B: VERIFICATION SCORES

TABLE 1
Summary of Number of Improved and Deteriorated Scores on Introduction of 3CV Physcis Package [Jan/Feb 95 (Jun/Aug 94)]

Verifying area	Improvement	Neutral	Detrimental
Global	12(12)	122(121)	1(2)
Area 2	2(5)	132(127)	1(3)
Northern Hemisphere	3(6)	130(123)	2(6)
Tropics	4(7)	128(124)	3(4)
Southern Hemisphere	3(10)	131(124)	1(1)

TABLE 2
Control Global Biases

	T+24	T+72	T+120
250hPa height (m)	-4.58	-12.09	-15.65
500hPa height (m)	-2.63	-5.98	-7.47
850hPa height (m)	-0.77	-2.00	-2.82
250hPa temperature (K)	-0.35	-0.60	-0.76
500hPa temperature (K)	-0.03	-0.21	-0.20
850hPa temperature (K)	-0.16	-0.41	-0.49

TABLE 3
3CV Package Global Biases

	T+24	T+72	T+120
250hPa height (m)	-4.77	-11.37	-13.76
500hPa height (m)	-2.57	-5.25	-6.26
850hPa height (m)	-0.73	-1.80	-2.52
250hPa temperature (K)	-0.37	-0.61	-0.72
500hPa temperature (K)	-0.03	-0.19	-0.16
850hPa temperature (K)	-0.16	-0.36	-0.42

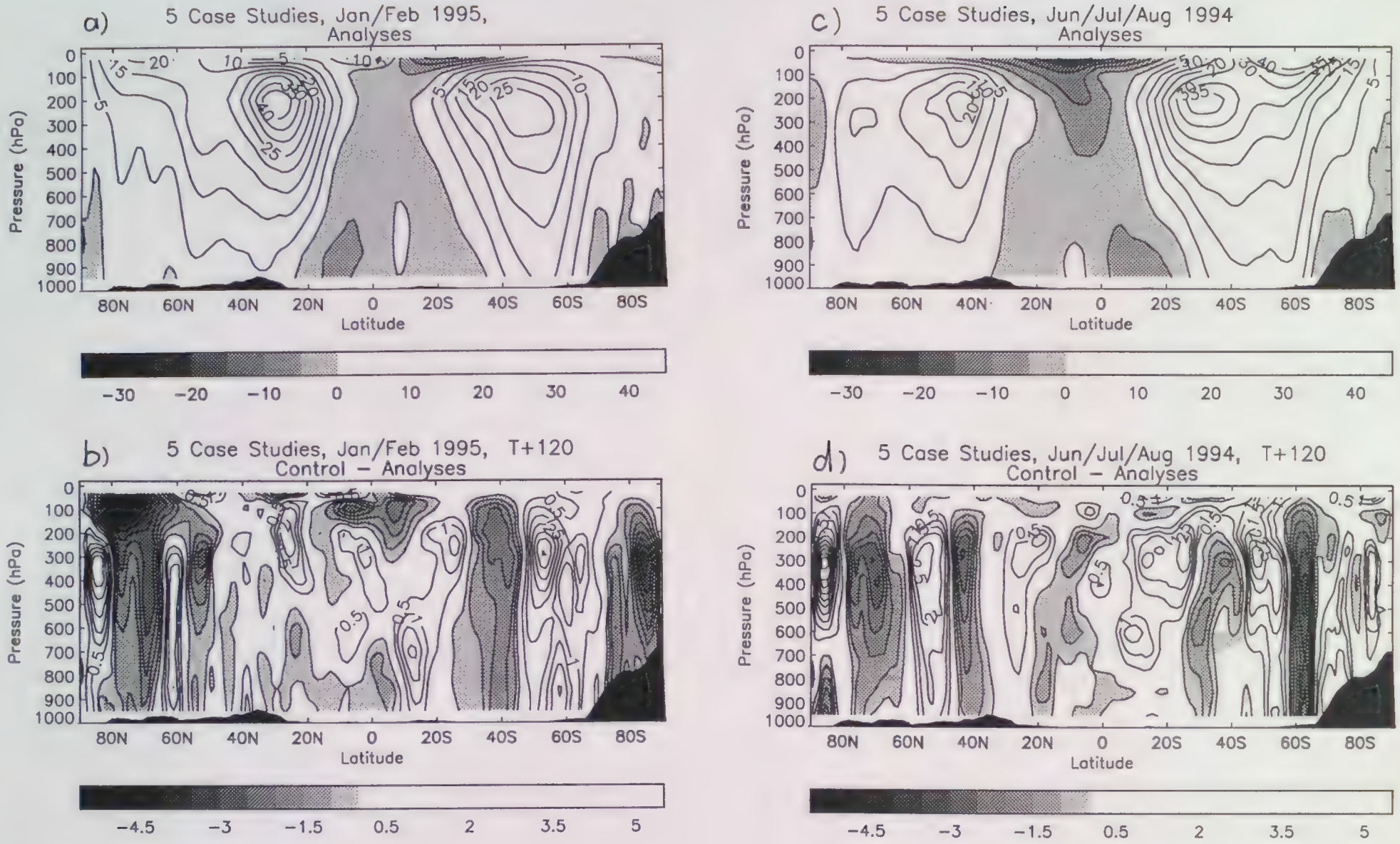

Figure 1 - Latitude-height (pressure) plots of zonally averaged zonal wind (a) Analysis at 00Z for 5 Jan/Feb 95 cases, (b) Mean error (Control - Analysis) at T+120 for 5 Jan/Feb 95 cases, (c) as (a) but for 5 Jun/Aug 94 cases, and (d) as (b) but for 5 Jun/Aug 94 cases.

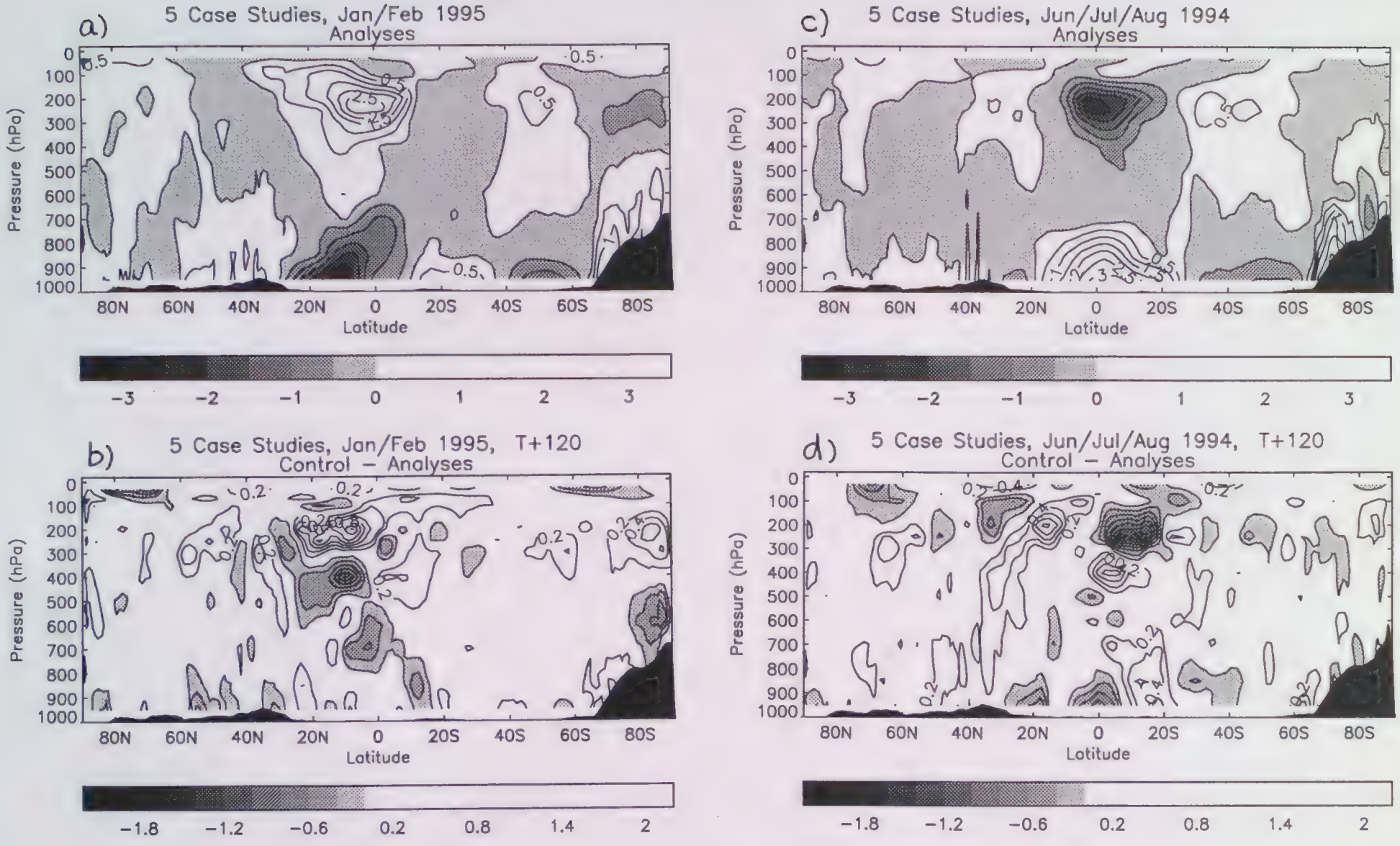

Figure 2 - Latitude-height (pressure) plots of zonally averaged meridional wind (a) Analysis at 00Z for 5 Jan/Feb 95 cases,(b) Mean error (Control - Analysis) at T+120 for 5 Jan/Feb 95 cases,(c) as (a) but for 5 Jun/Aug 94 cases, and (d) as (b) but for 5 Jun/Aug 94 cases.

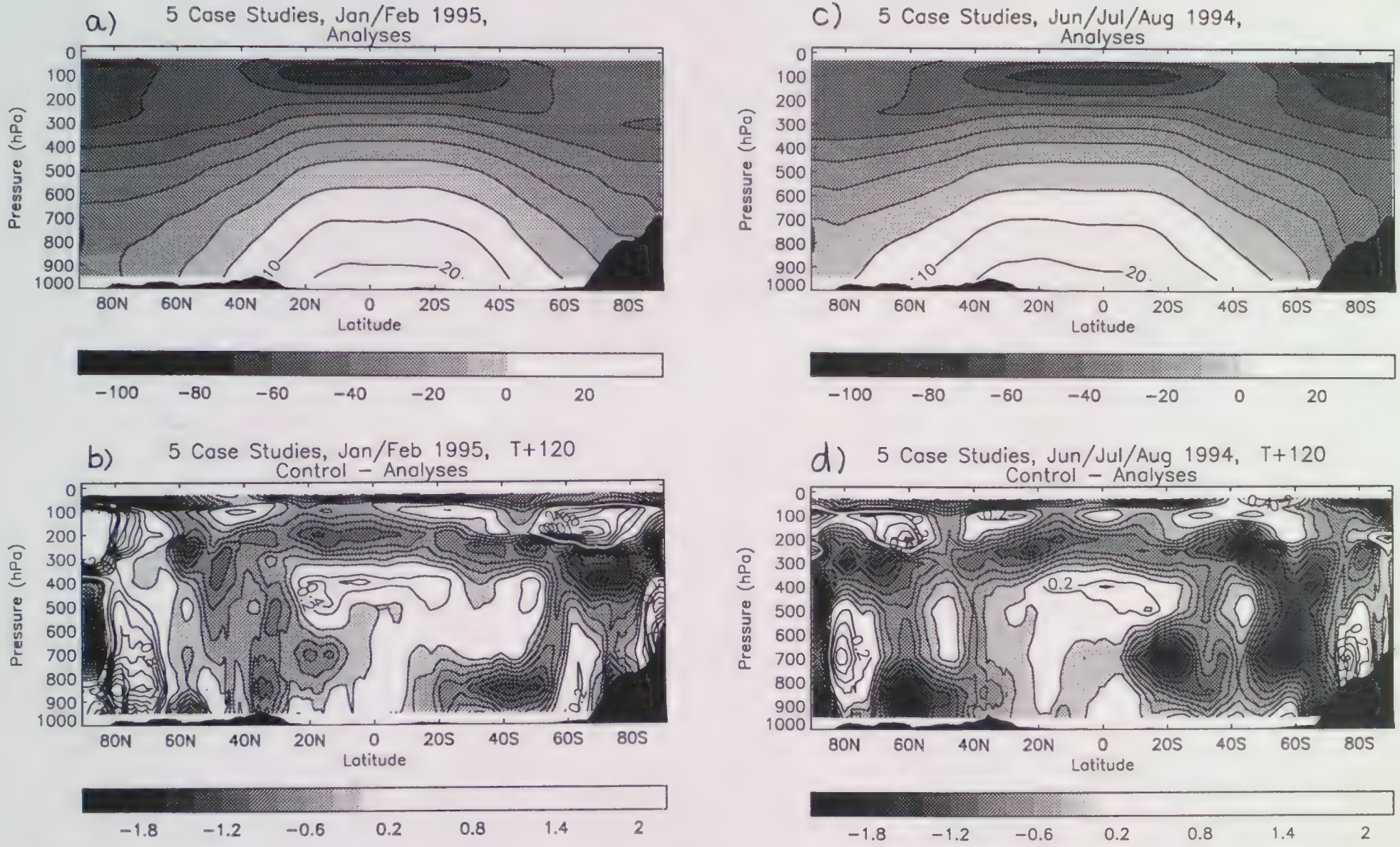

Figure 3 - Latitude-height (pressure) plots of zonally averaged Temperature (a) Analysis at 00Z for 5 Jan/Feb 95 cases,(b) Mean error (Control-Analysis) at T+120 for 5 Jan/Feb 95 cases,(c) as (a) but for 5 Jun/Aug 94 cases, and (d) as (b) but for 5 Jun/Aug 94 cases.

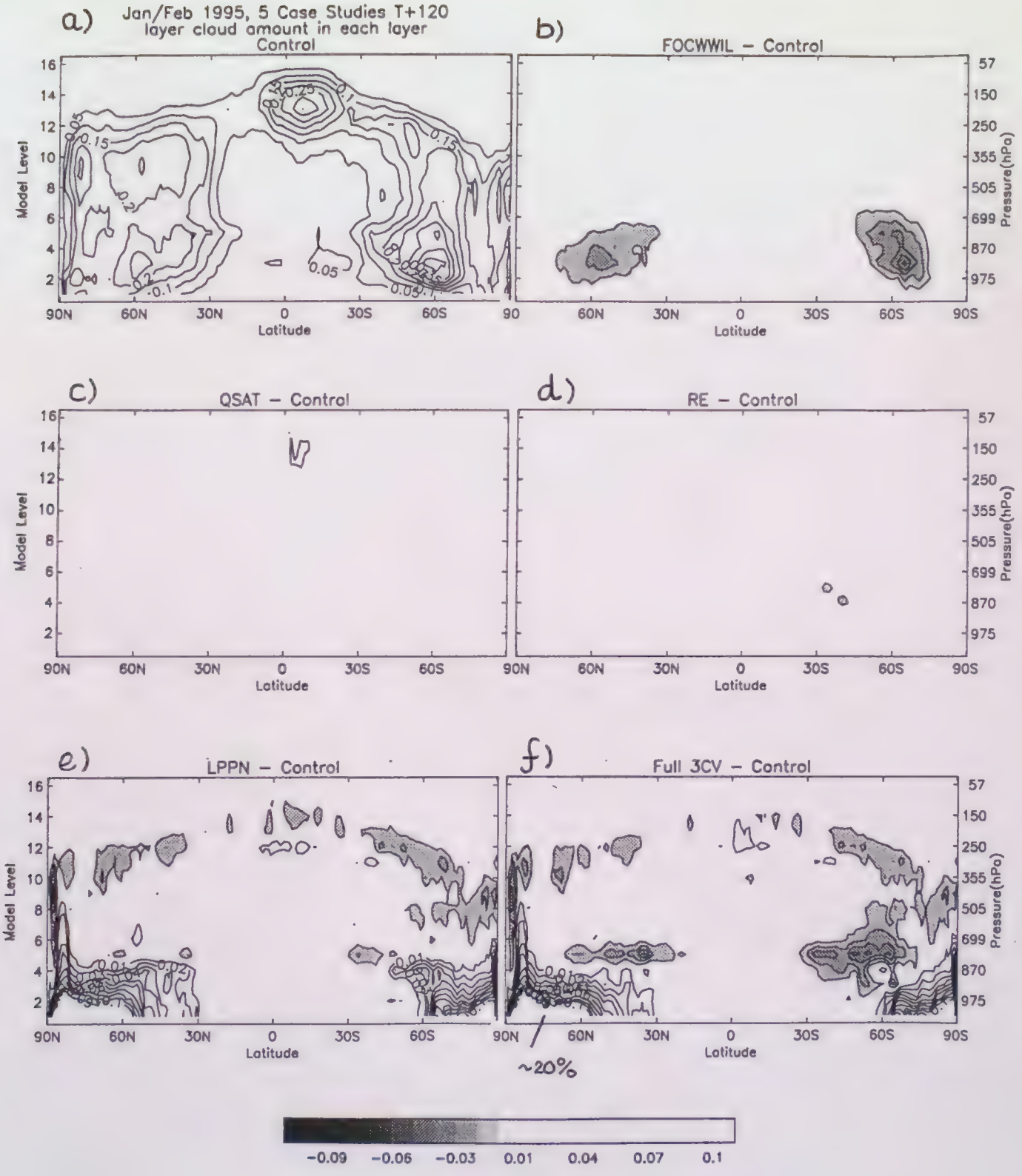

Figure 4 - Latitude-height (pressure) plots of zonally averaged cloud for Jan/Feb 95 cases. (a) Control at T+120, (b) FOCWWIL - Control, (c) QSAT - Control, (d) RE - Control, (e) LPPN - Control, (f) Full 3CV - Control.

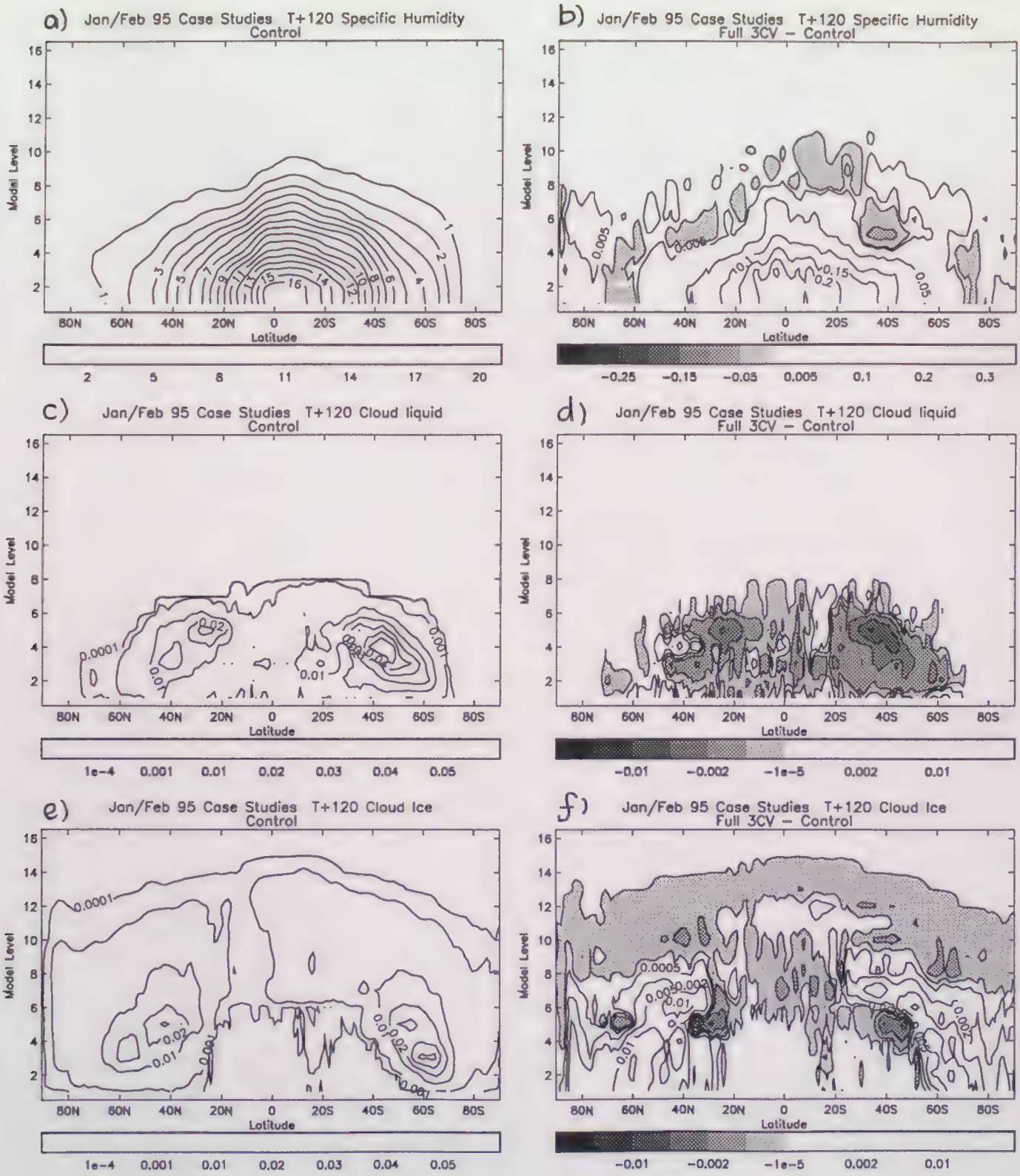

Figure 4B - Impact of Full 3CV on moisture variables at T+120 for Jan/Feb cases (a) specific humidity: Control , (b) specific humidity: Full 3CV - Control (c) Cloud liquid water: Control, (d) Cloud liquid water: Full 3CV - Control, (e) Cloud ice: Control, (f) Cloud ice: Full 3CV - Control. Units are g/kg

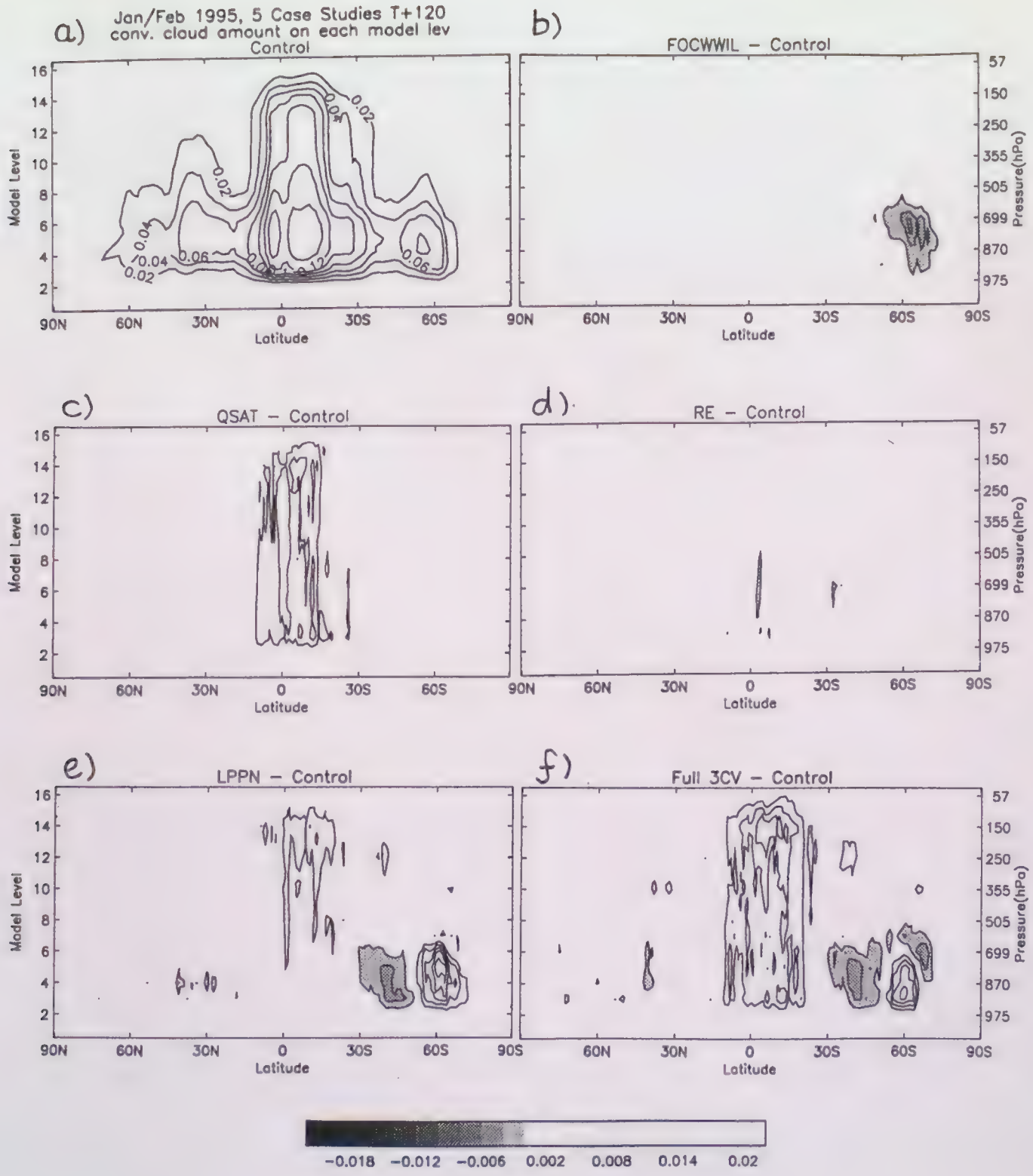

Figure 5 - As figure 4 but for convective cloud.

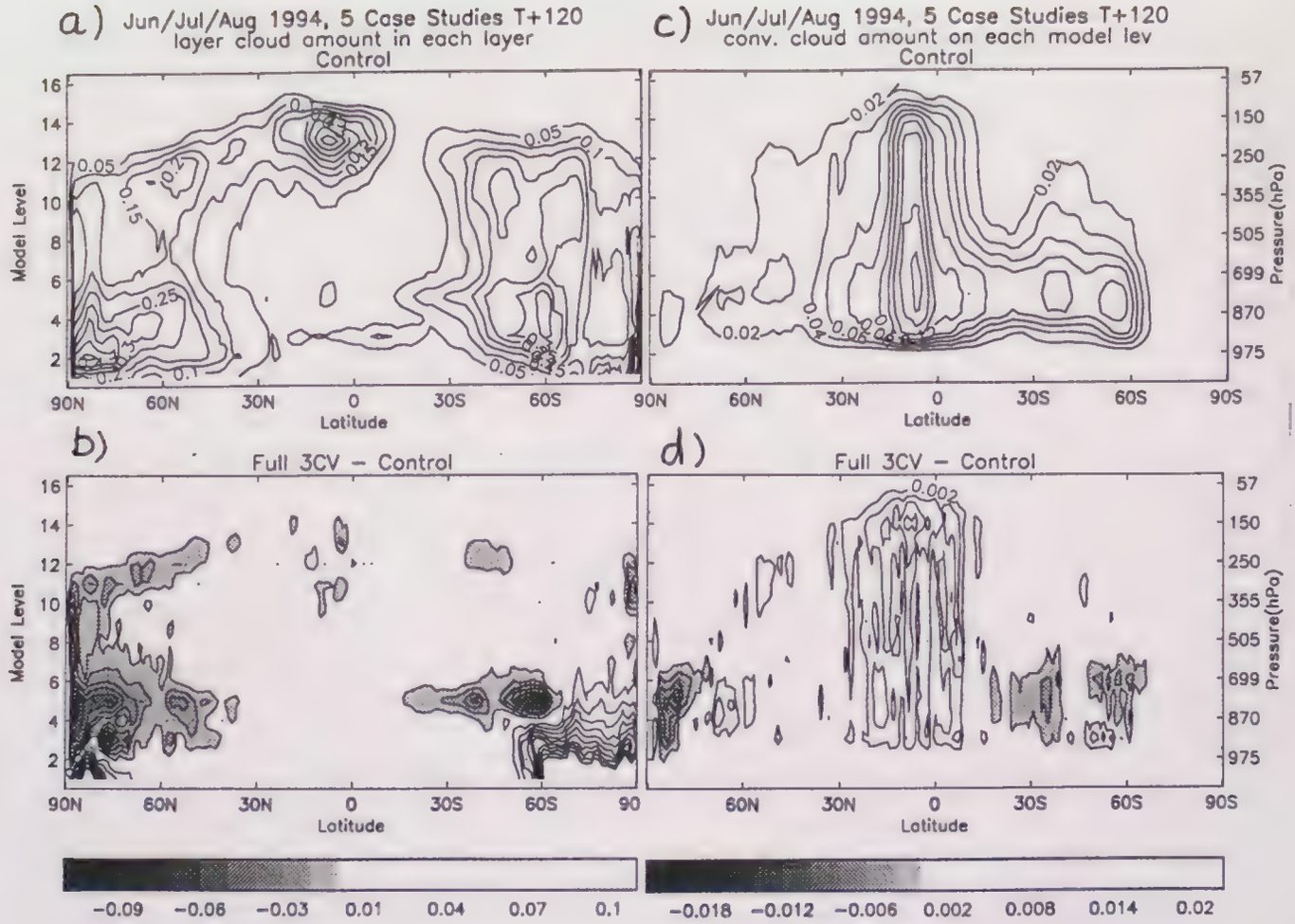

Figure 6 - Latitude-height (pressure) plots of zonally averaged cloud for Jun/Aug 94 cases. (a) Control layer cloud at T+120, (b) Full 3CV - Control layer cloud, (c) Control convective cloud at T+120, (d) Full 3CV - Control convective cloud.

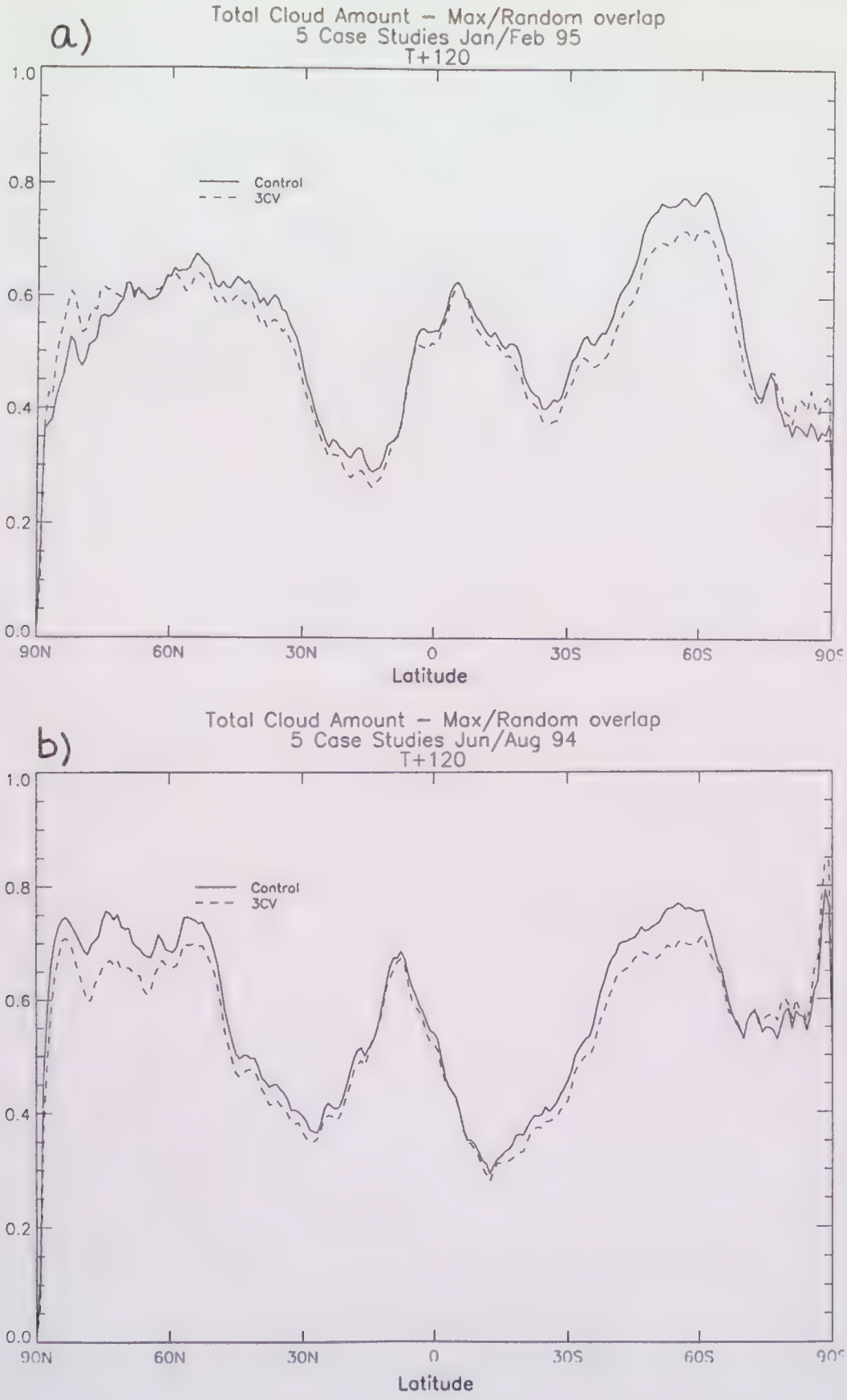

Figure 7 - Zonally averaged latitudinal profile of total cloud amount (max/random overlap) at T+120 for (a) Jan/Feb 95 cases, (b) Jun/Aug 94 cases.

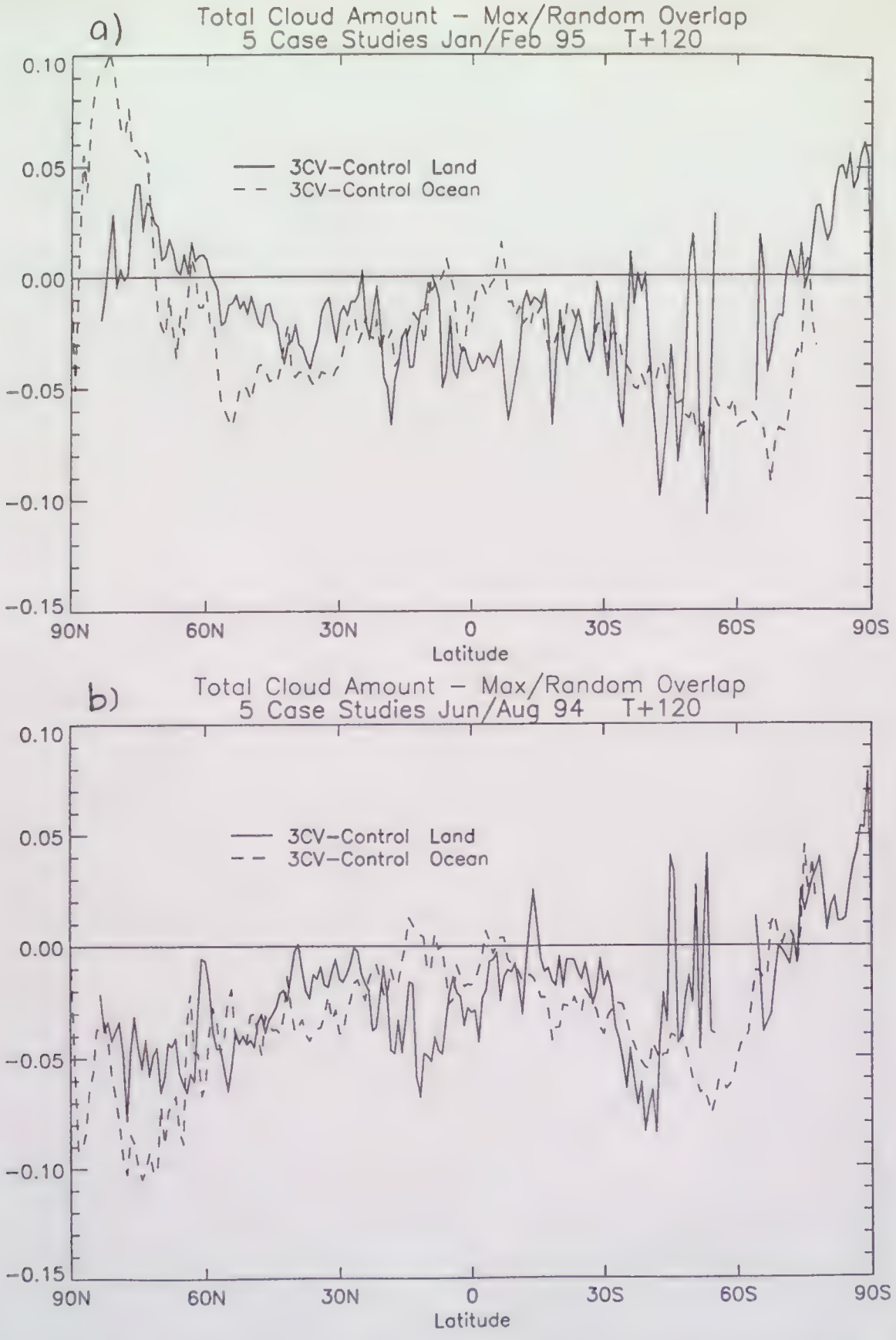

Figure 8 - Zonally averaged latitudinal profile of total cloud amount (max/random overlap) differences (3CV - Control) at T+120 for land and ocean points (a) Jan/Feb 95cases, (b) Jun/Aug 94 cases.

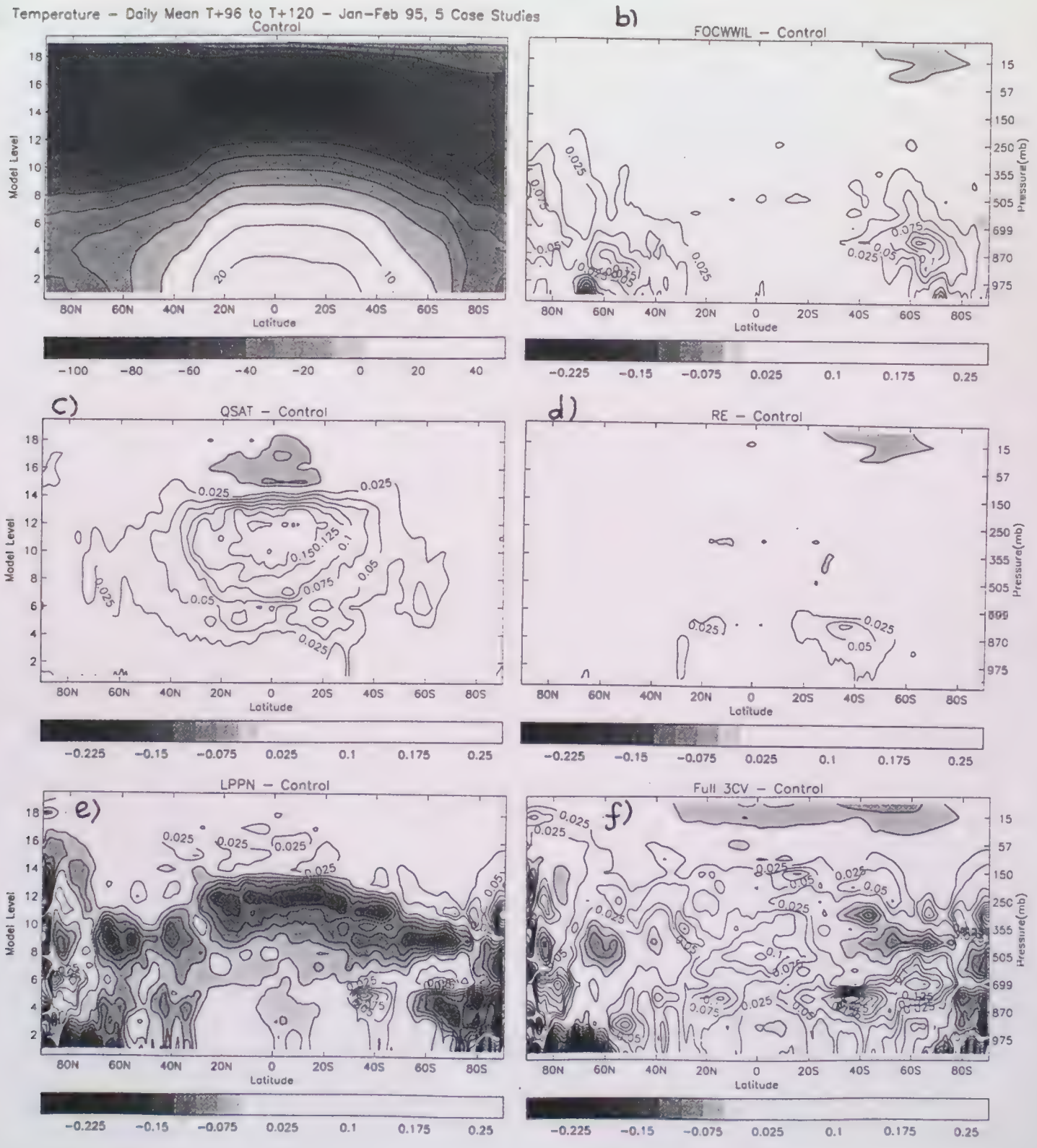

Figure 9 - Zonally averaged latitudinal profile of temperature averaged over T+96 to T+120 for Jan/Feb 95 cases (a) Control, (b) FOCWWIL - Control, (c) QSAT - Control, (d) RE - Control, (e) LPPN - Control, and (f) Full 3CV - Control. Units are K.

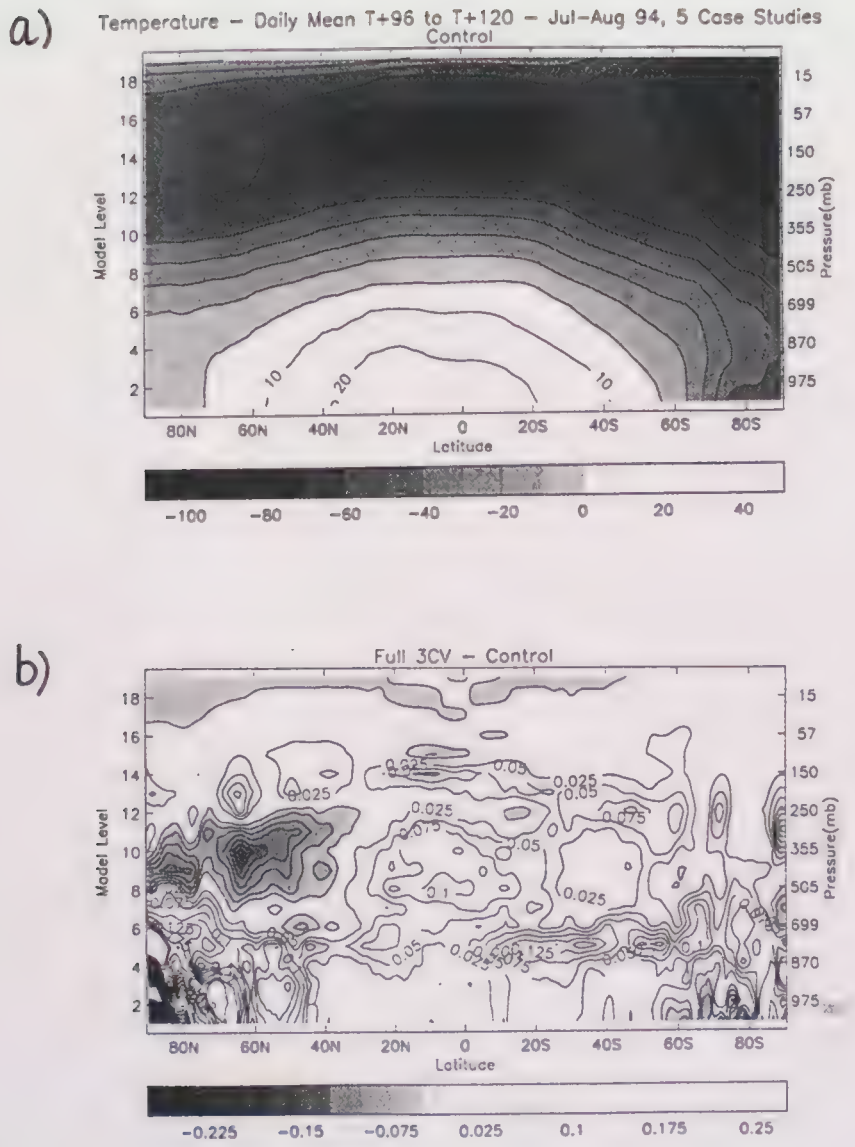

Figure 10 - Zonally averaged latitudinal profile of temperature averaged over T+96 to T+120 for Jun/Aug 94 cases (a) Control, (b) Full 3CV - Control. Units are K.

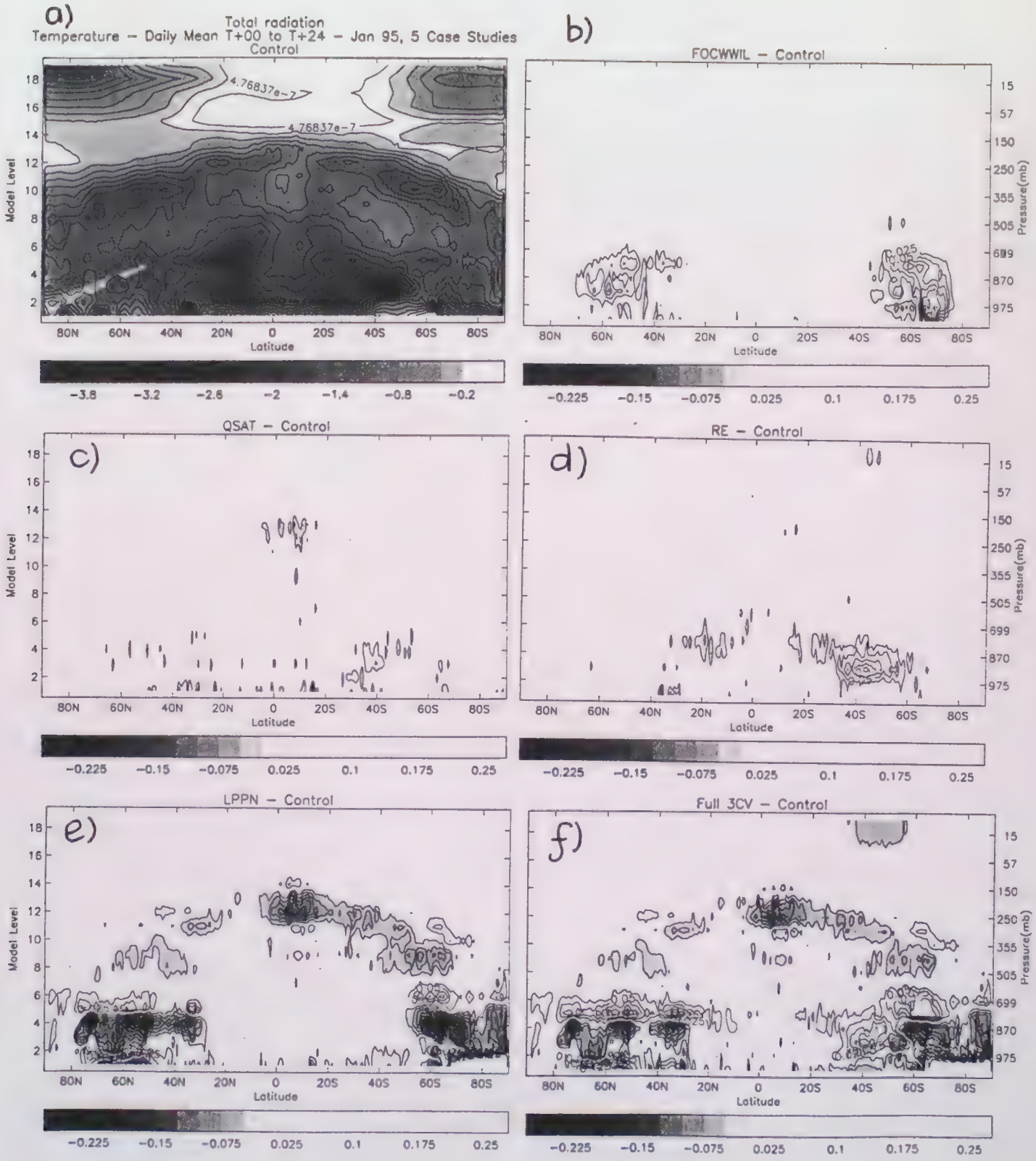

Figure 11 - Zonally averaged latitudinal profile of radaitive heating increments averaged over T+00 to T+24 for Jan/Feb 95 cases (a) Control, (b) FOCWWIL - Control, (c) QSAT - Control, (d) RE - Control, (e) LPPN - Control, and (f) Full 3CV - Control. Units are K/day.

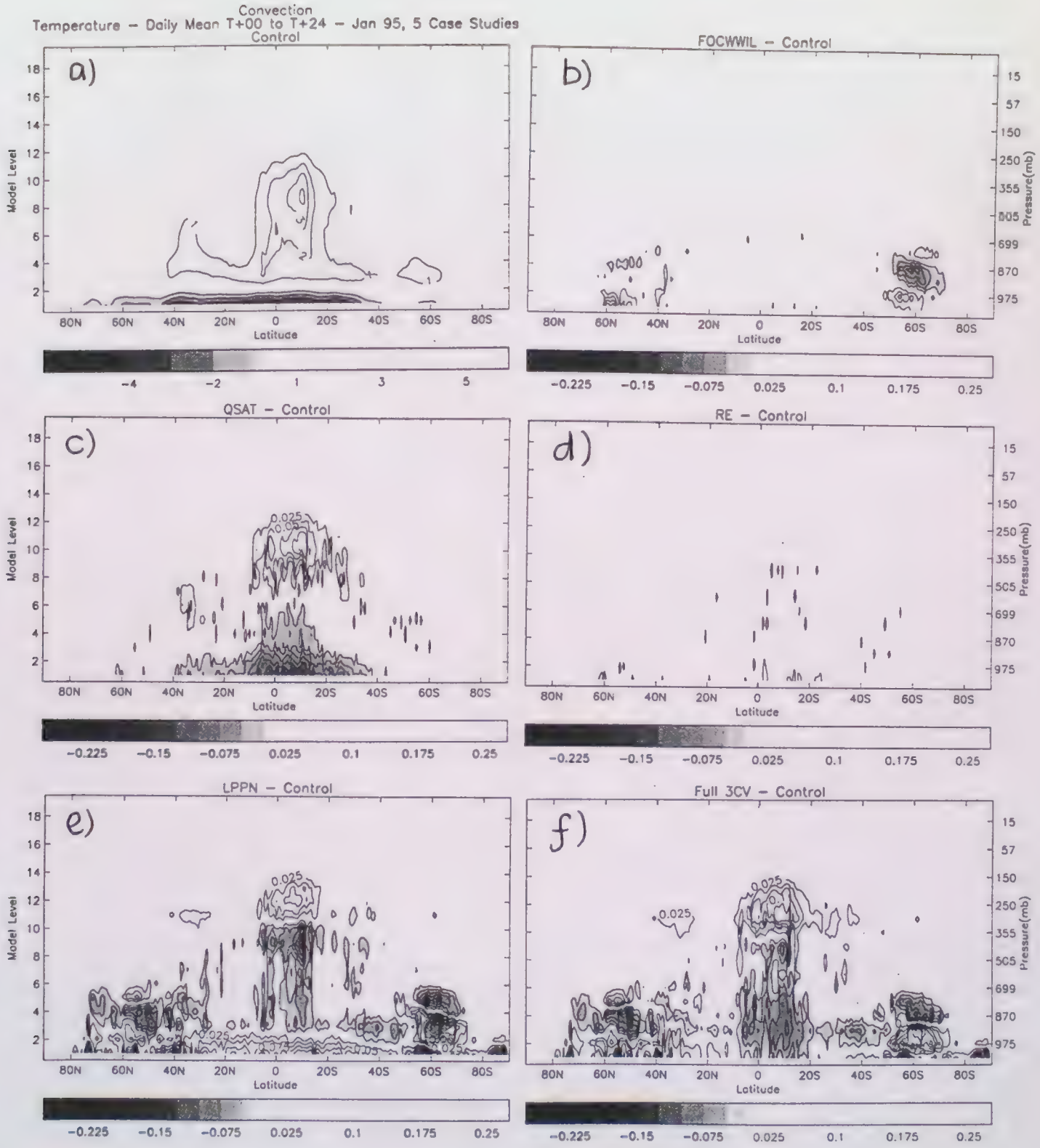

Figure 12 - As figure 11 but for convective heating increments. Units are K/day.

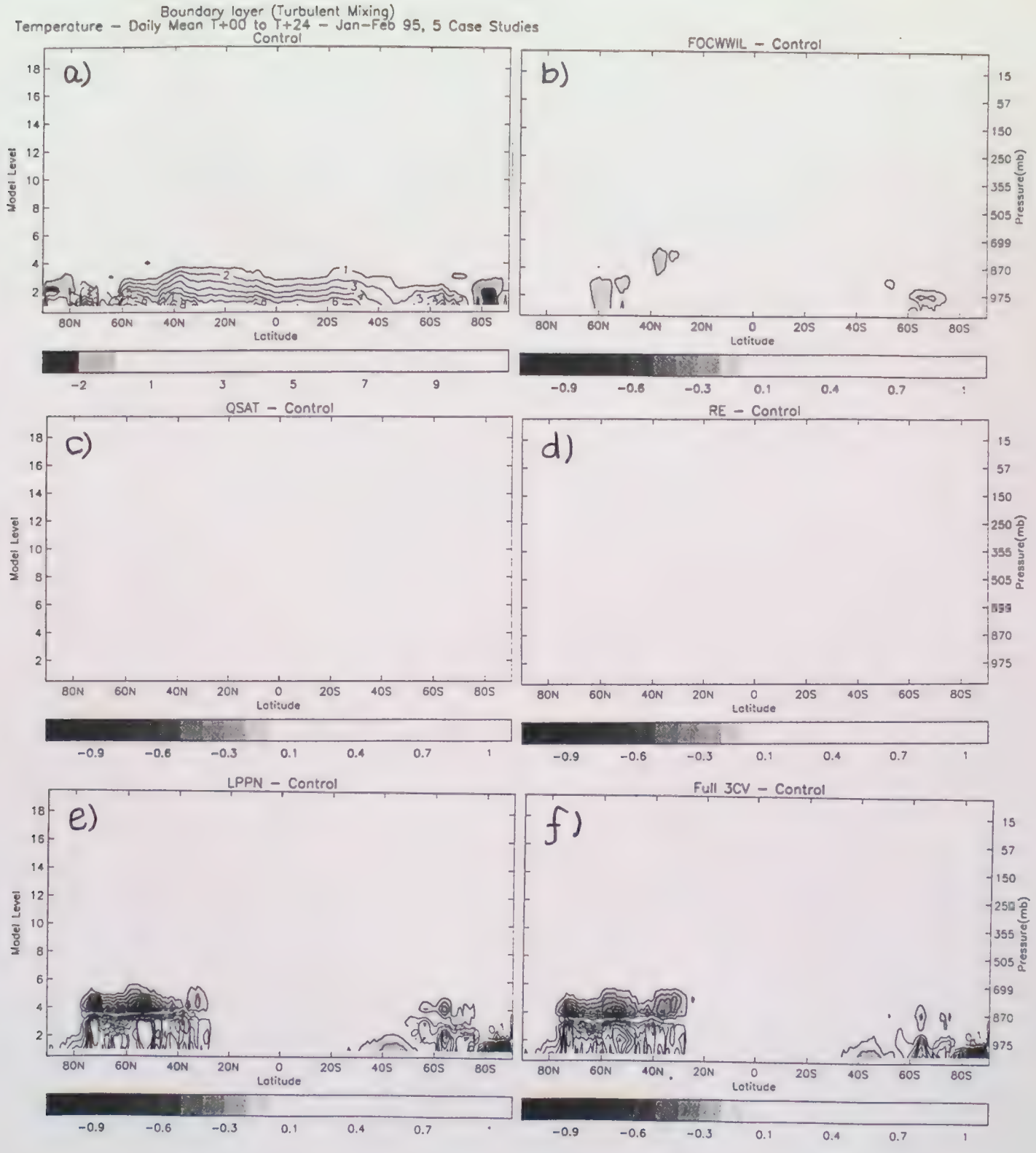

Figure 13 - As figure 11 but for boundary layer heating increments. Units are K/day.

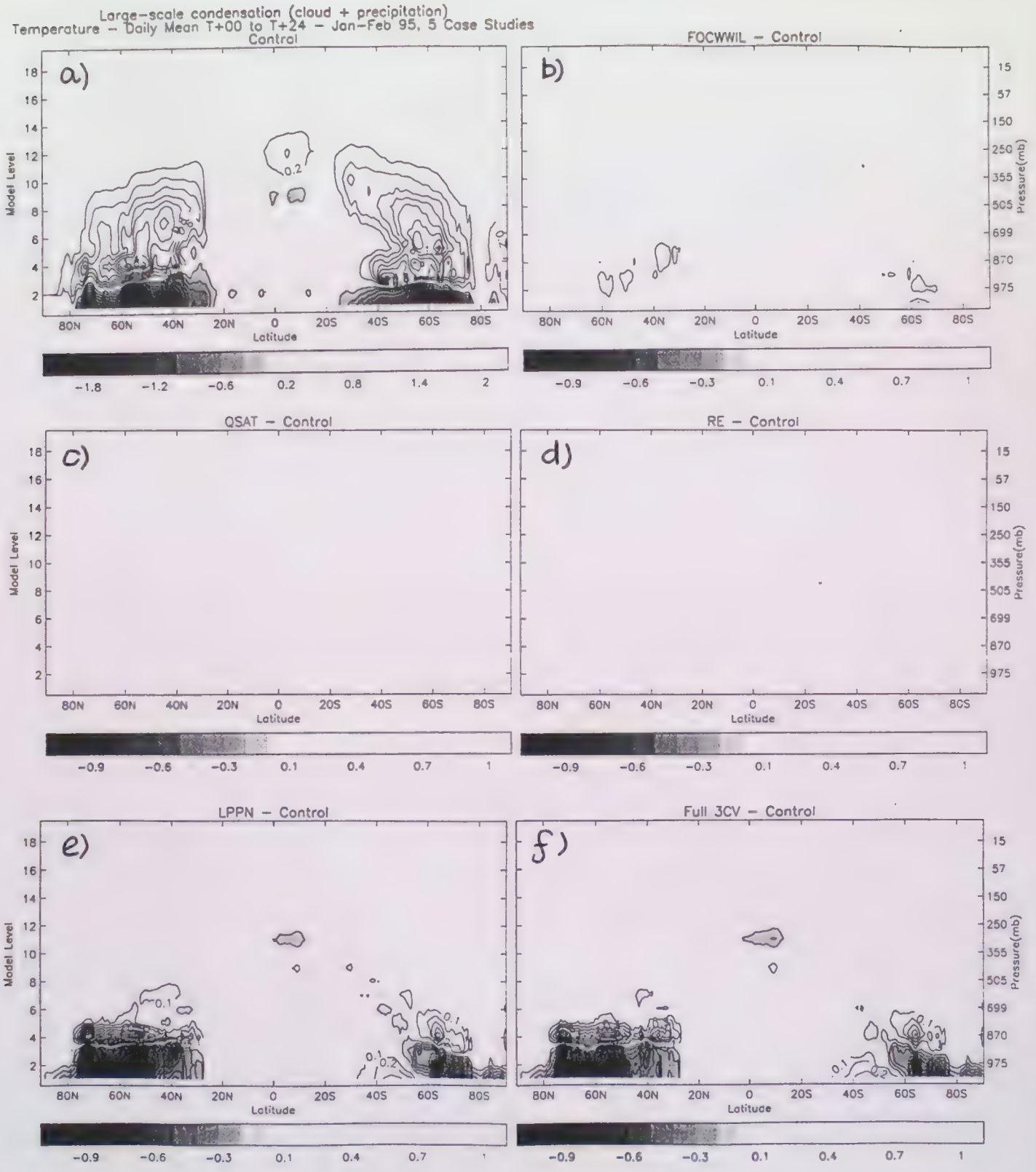

Figure 14 - As figure 11 but for large scale condensation (cloud + precipiation) heating increments. Units are K/day.

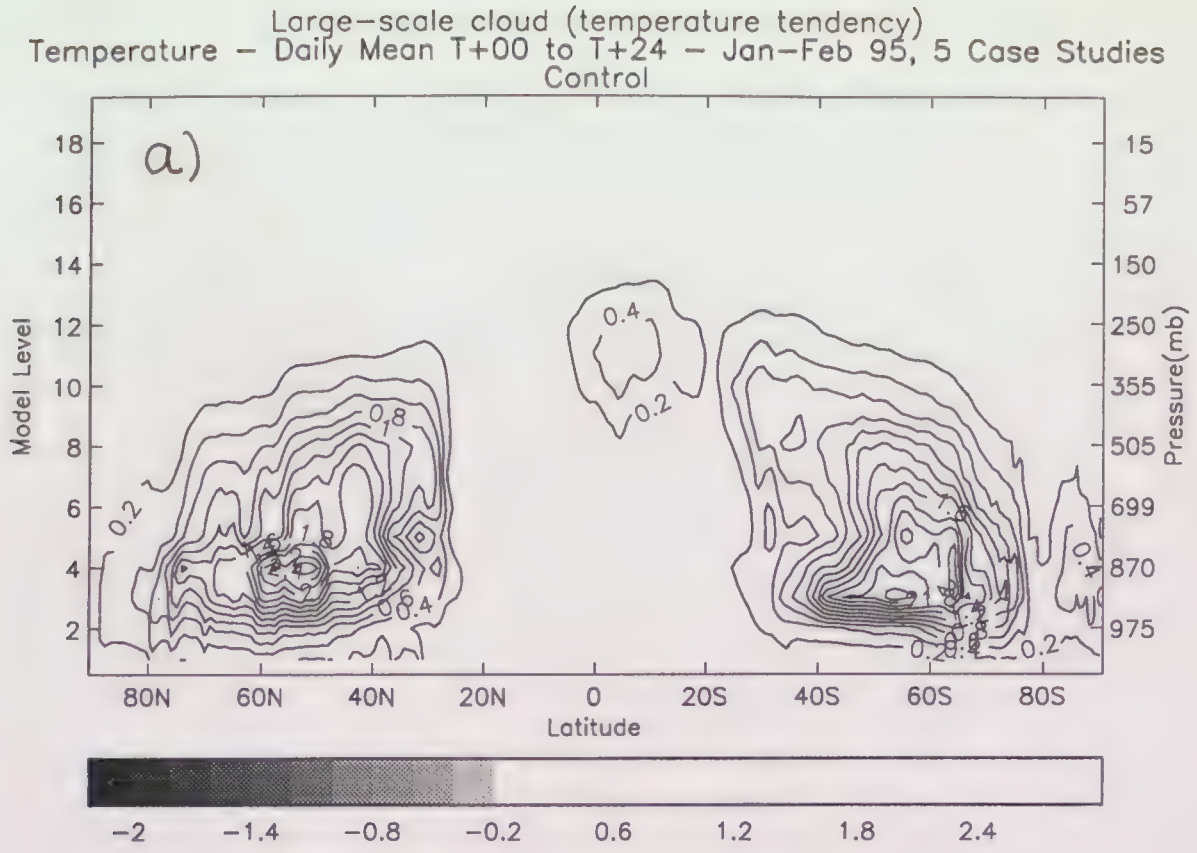

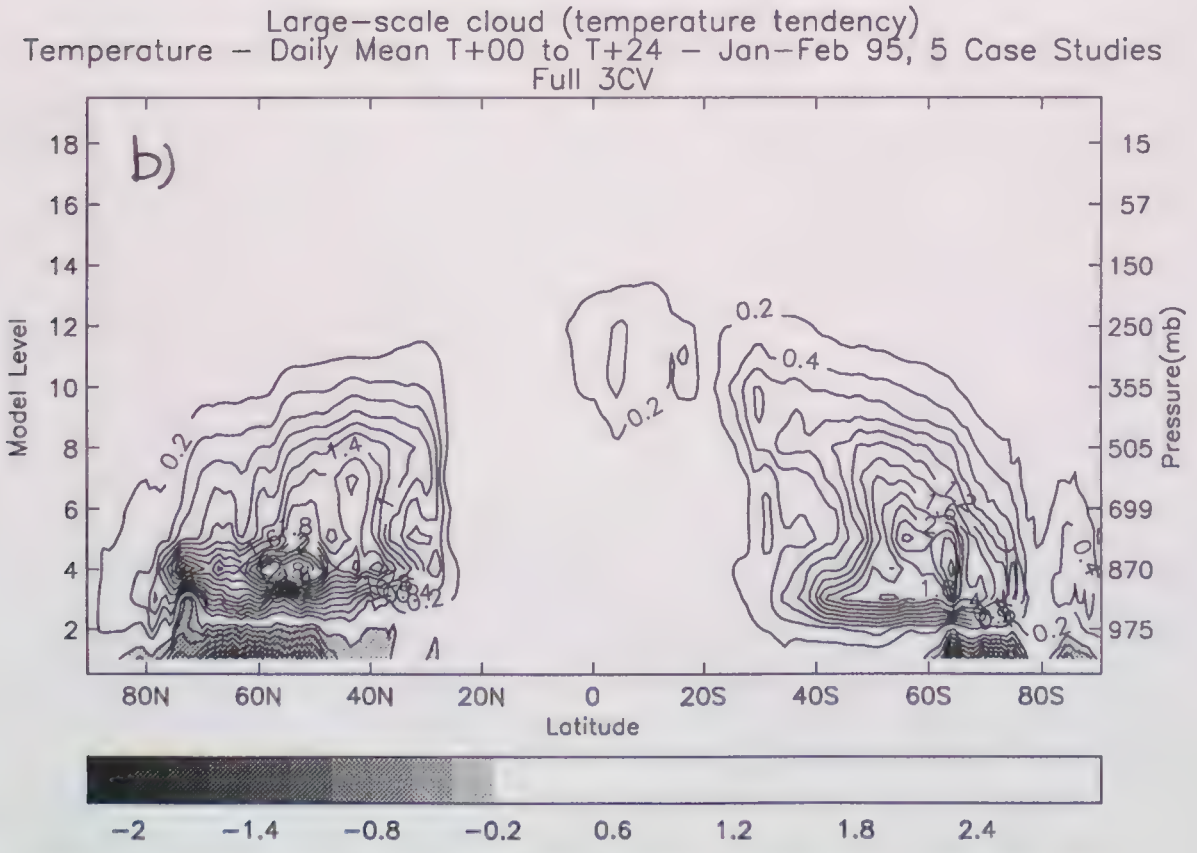

Figure 14B - Zonally averaged latitudinal profile of heating increments due to large scale cloud averaged over T+00 to T+24 for Jan/Feb 95 cases (a) Control, (b) Full 3CV . Units are K/day.

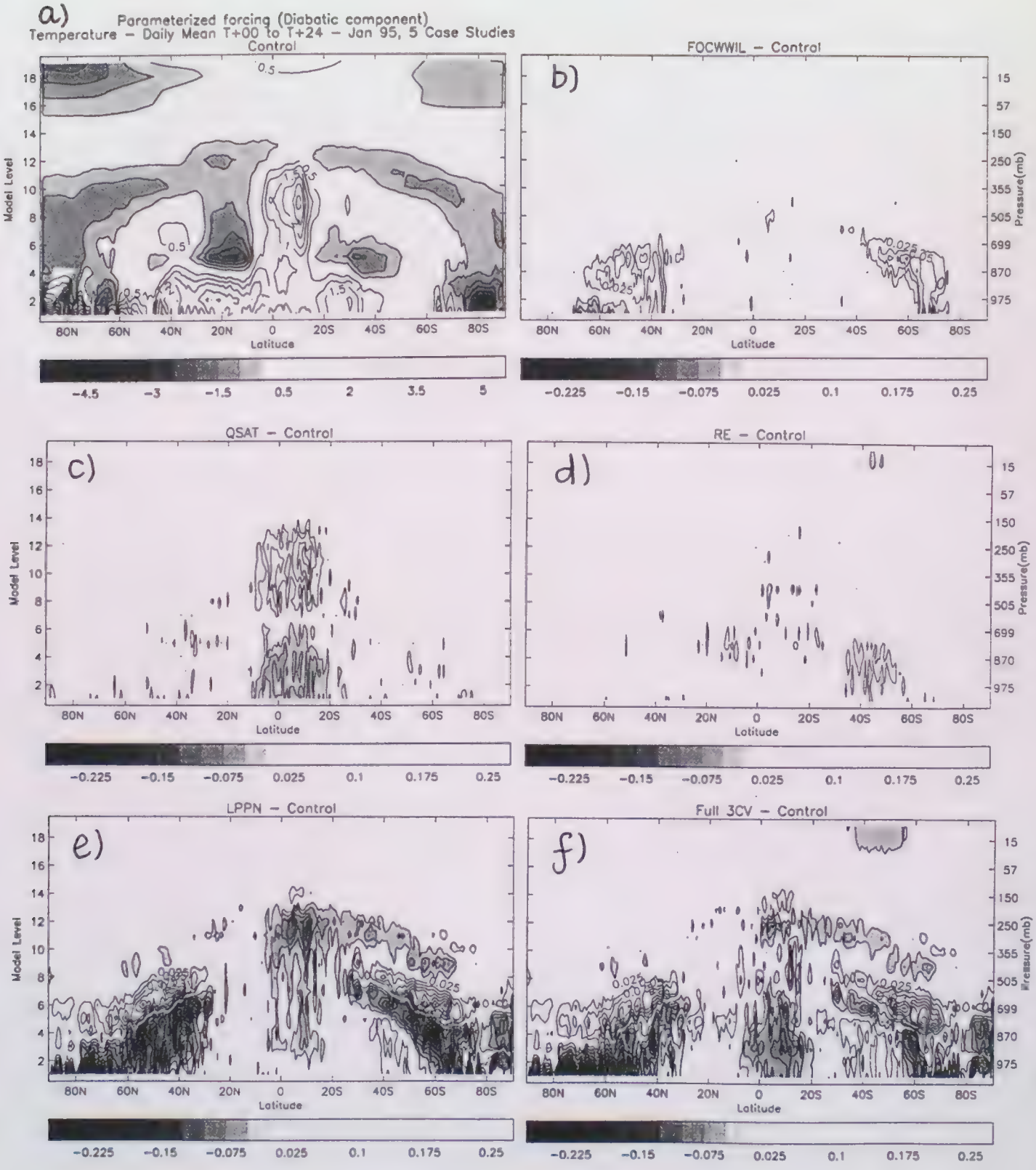

Figure 15 - As figure 11 but for total parametrized heating increments (Diabatic heating). Units are K/day.

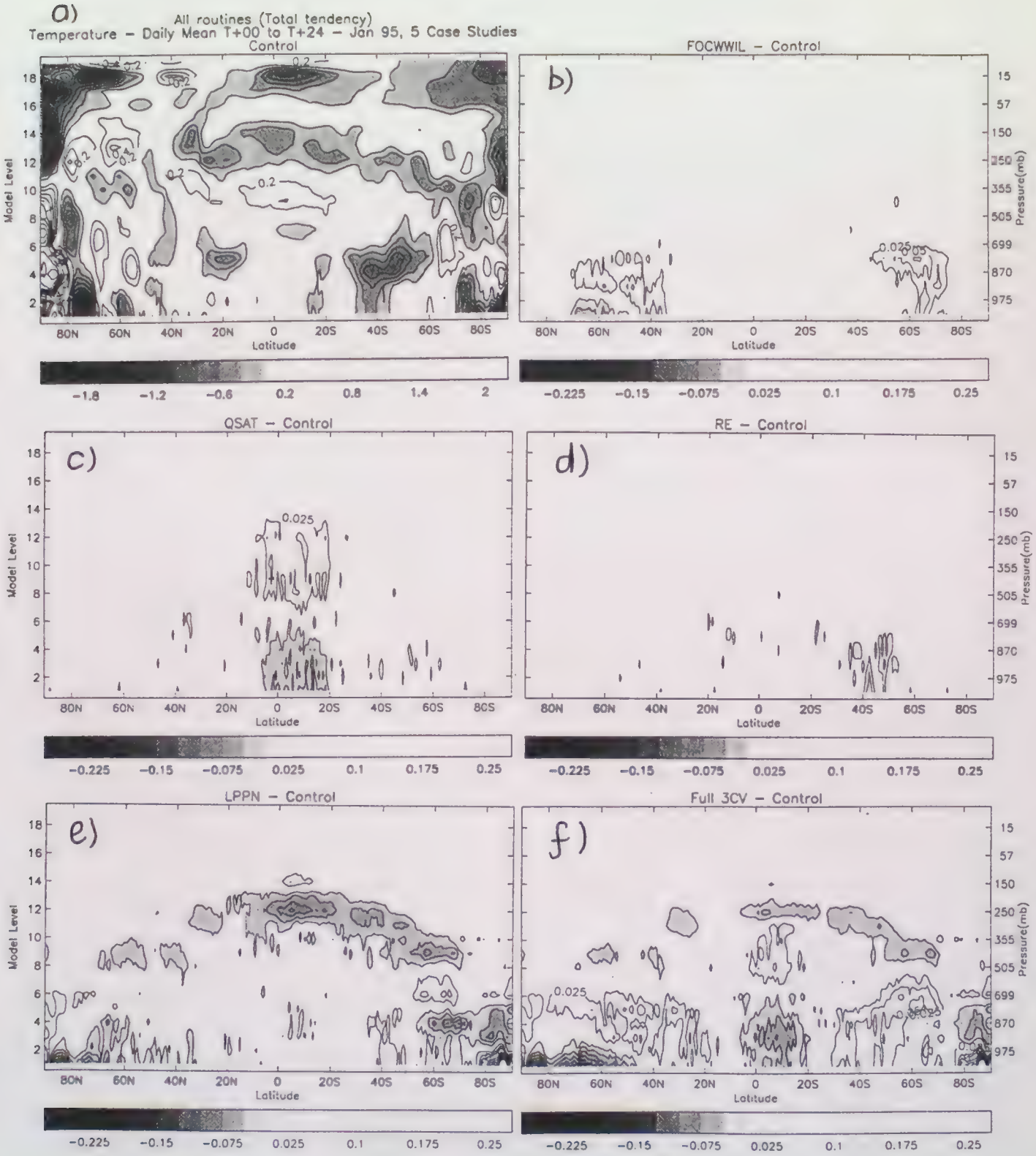

Figure 16 - As figure 11 but for total (parametrized + dynamical) heating increments. Units are K/day.

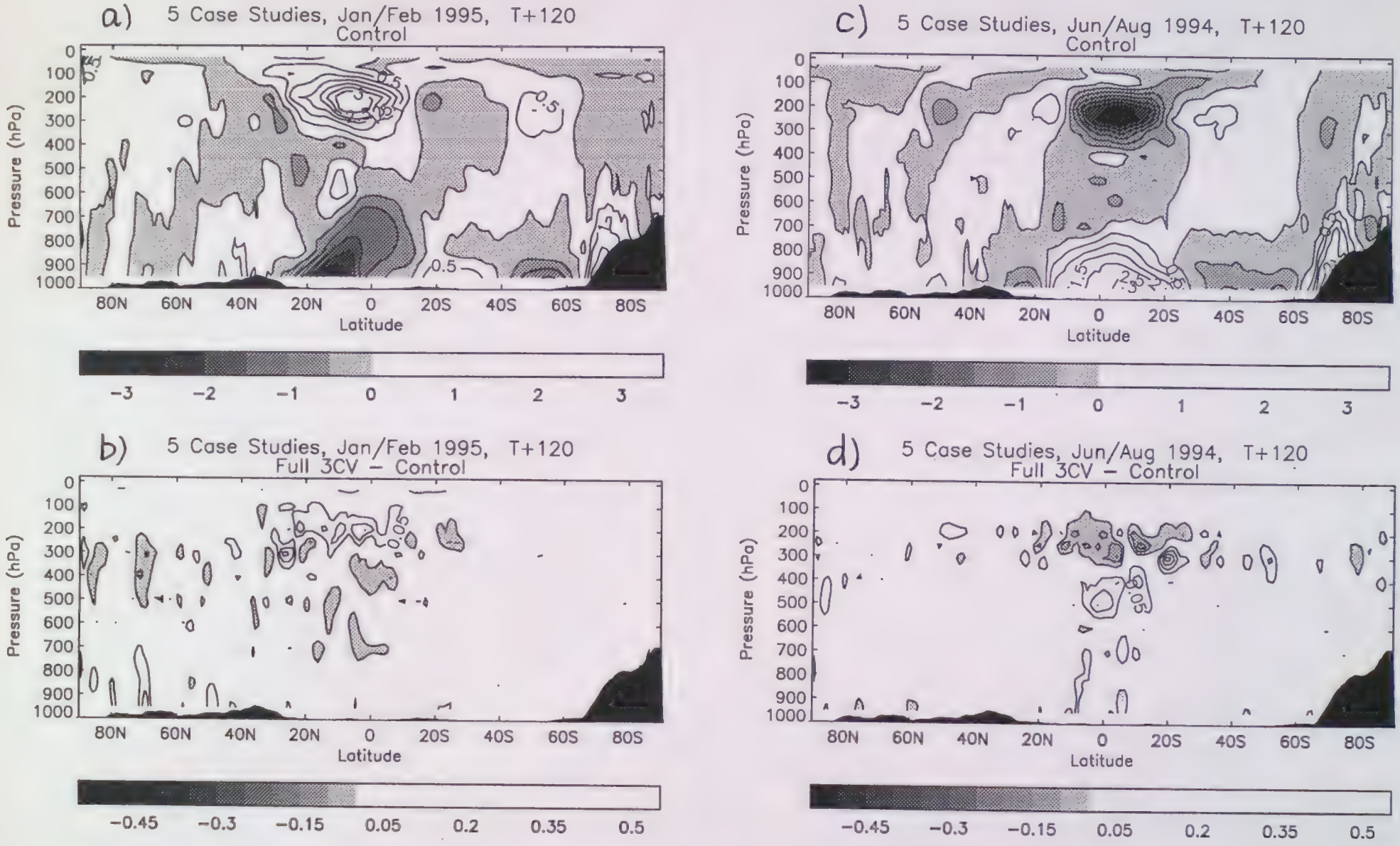

Figure 17 - Latitude-height (pressure) plots of zonally averaged meridional wind at T+120 for (a) Control for 5 Jan/Feb 95 cases, (b) Full 3CV - Control for 5 Jan/Feb 95 cases,(c) as (a) but for 5 Jun/Aug 94 cases, and (d) as (b) but for 5 Jun/Aug 94 cases.

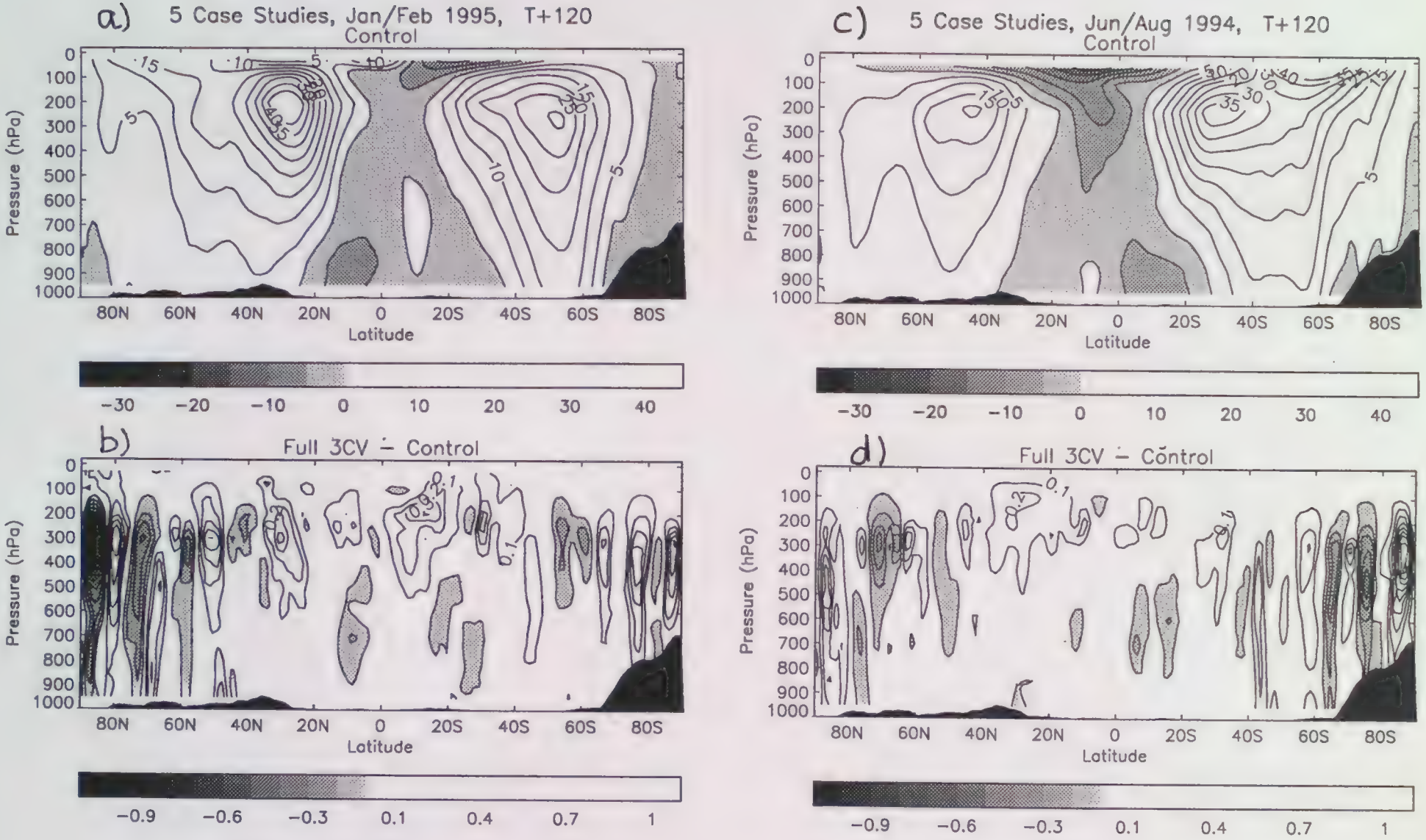

Figure 18 - Latitude-height (pressure) plots of zonally averaged zonal wind at T+120 for (a) Control for 5 Jan/Feb 95 cases, (b) Full 3CV - Control for 5 Jan/Feb 95 cases,(c) as (a) but for 5 Jun/Aug 94 cases, and (d) as (b) but for 5 Jun/Aug 94 cases.

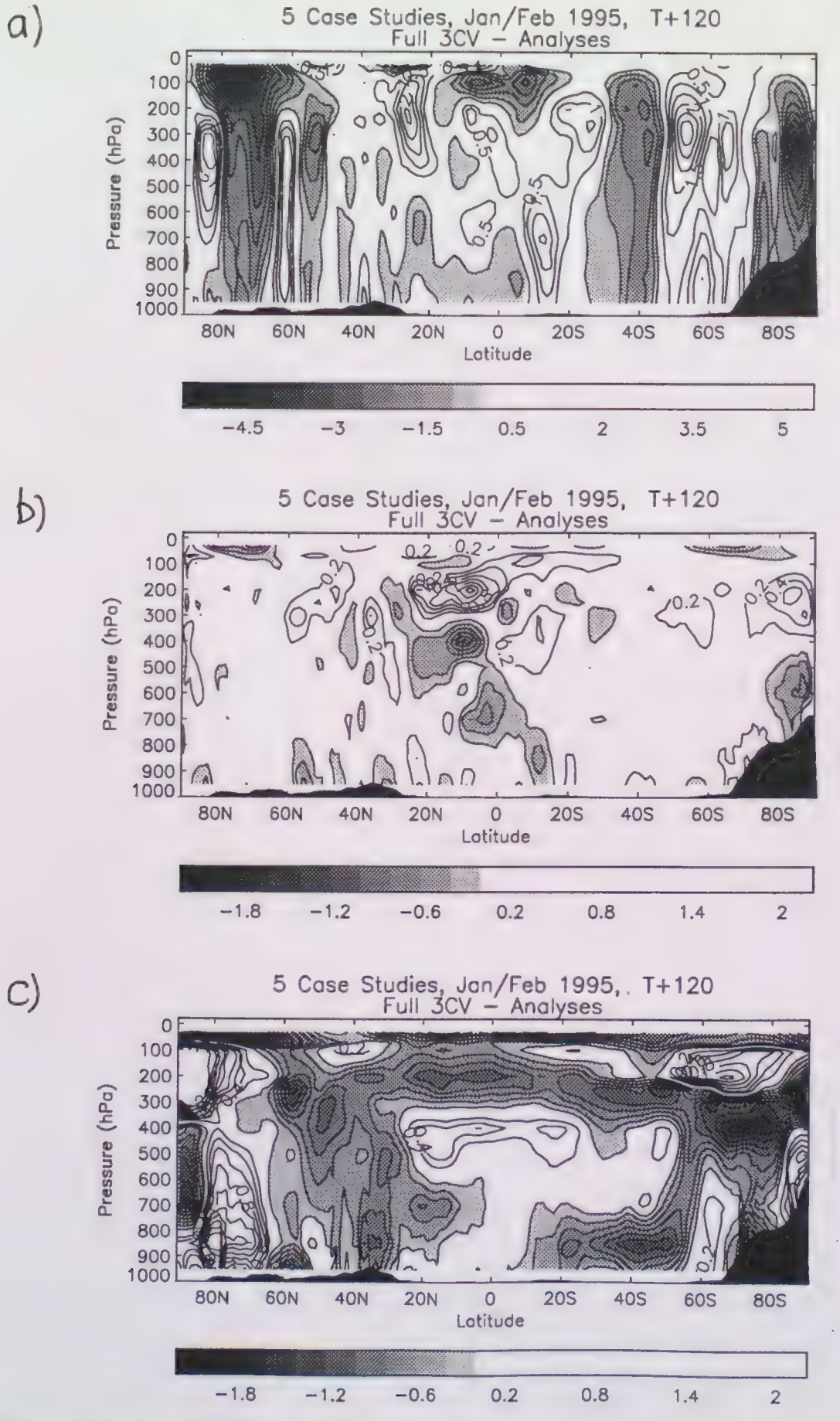

Figure 19 - Latitude-height (pressure) plots of zonally averaged mean errors (forecast - analysis) at T+120 for 5 Jan/Feb 95 cases of Full 3CV forecasts (a) Zonal wind (b) meridional wind,(c) temperature.

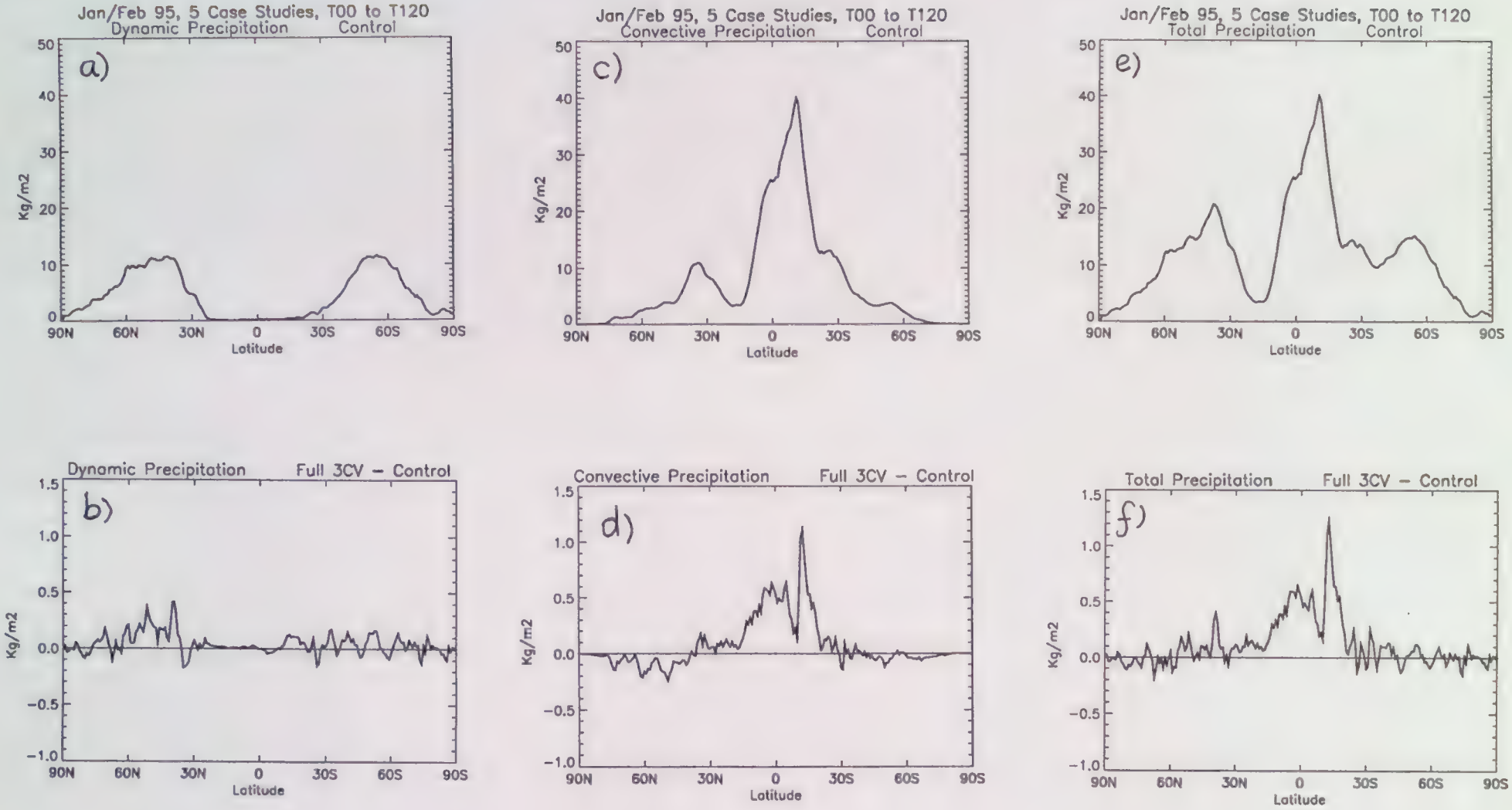

Figure 20 - Zonally averaged precipitation for Jan/Feb 95 cases accumulated over T+00 to T+120 for Jan/Feb 95 cases (a) Dynamic precipitation : Control, (b) Dynamic precipitation : 3CV - Control, (c) Convective precipitation - Control (d) Convective precipitation :3CV - Control, (e) Total precipitation: Control (f) Total precipitation :3CV - Control.

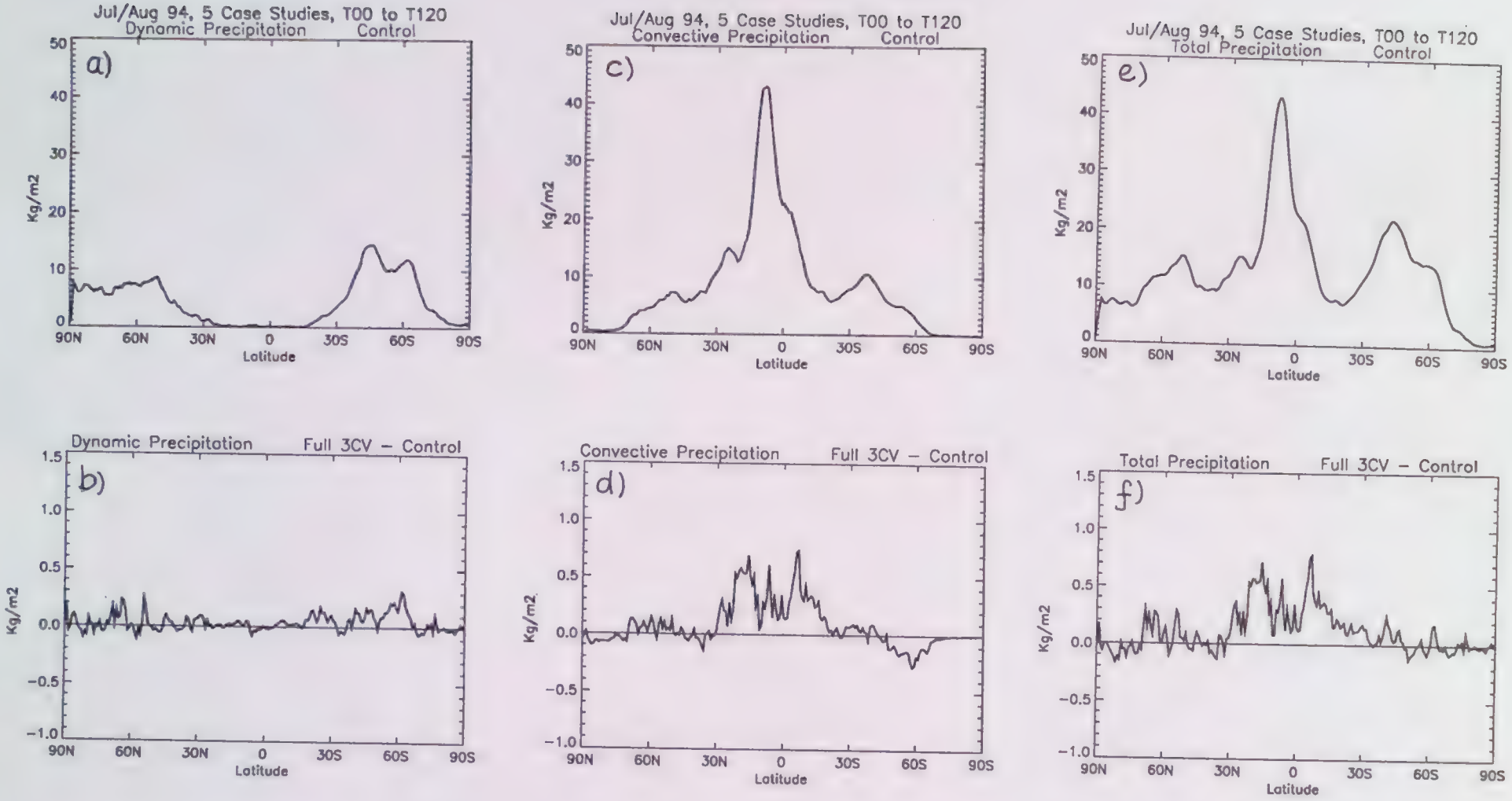

Figure 21 - As figure 20 but for Jun/Aug 94 cases.

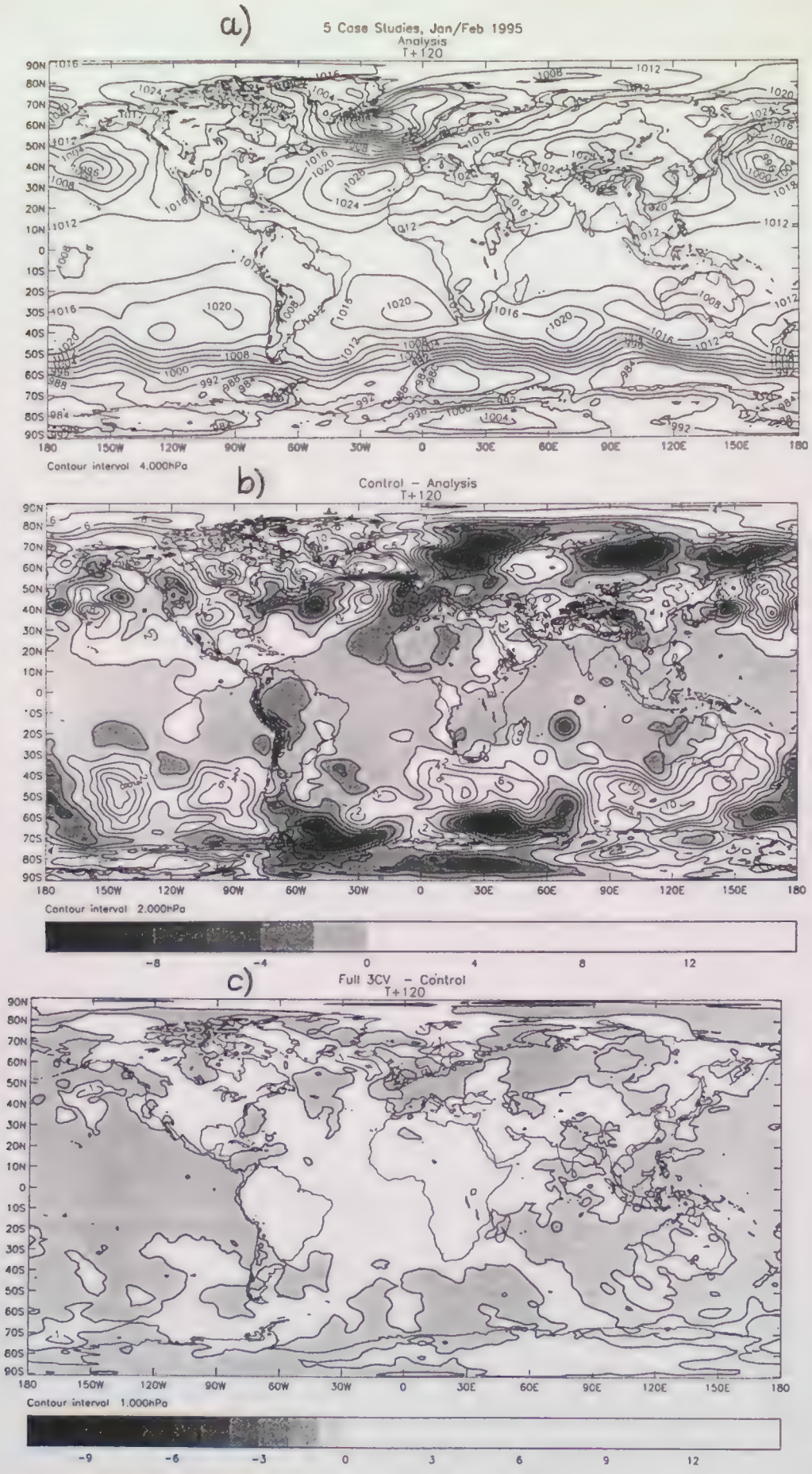

Figure 22 - MSLP averaged over 5 case studies from Jan/Feb 1995, (a) Analysis, (b) Control - Analysis T+120, (c) Full 3CV - Control.

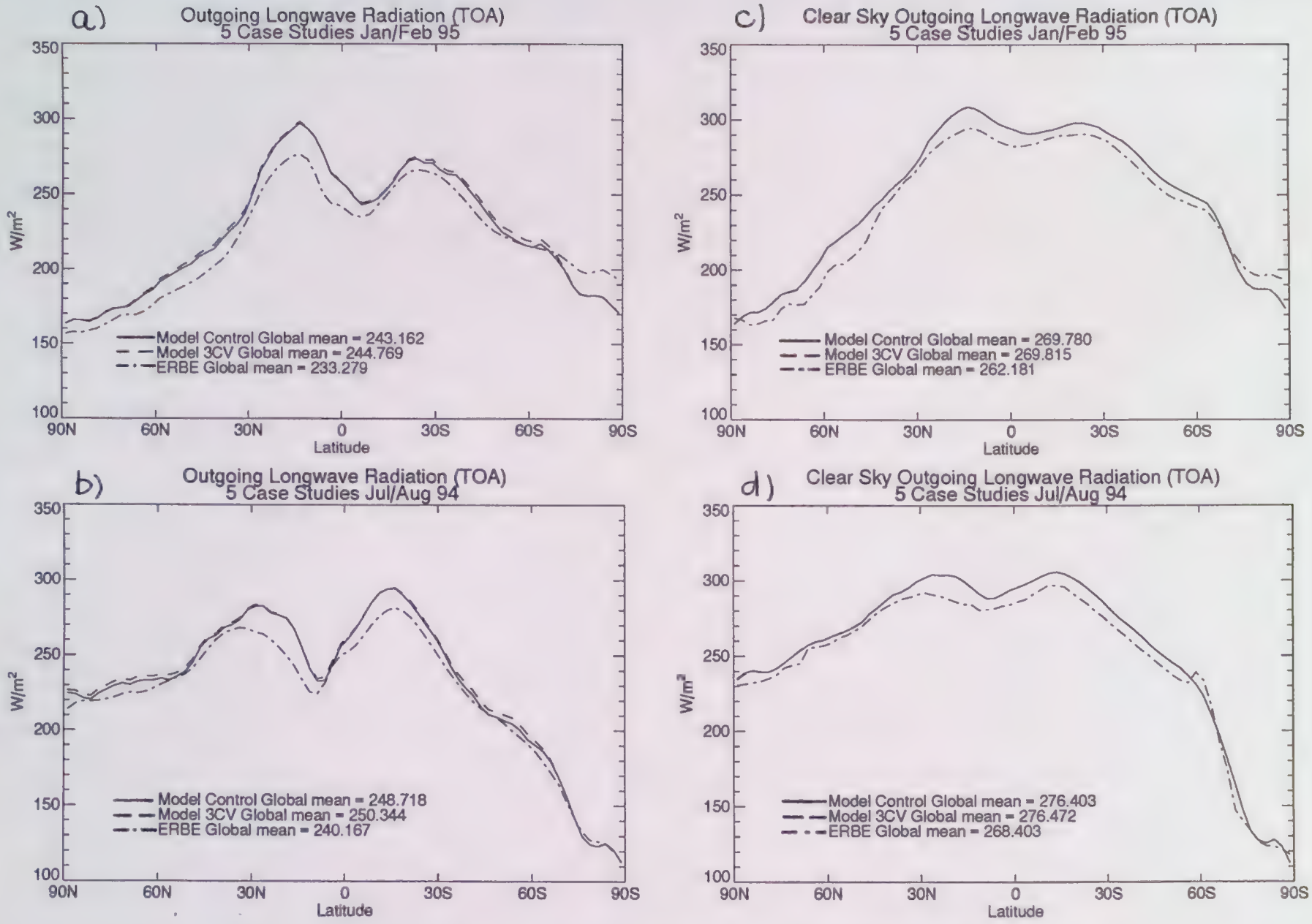

Figure 23 - Zonally averaged model TOA radiative flux (T+96 to T+120) comparisons with ERBE data (1988), (a) OLR Jan/Feb, (b) OLR Jun/Aug, (c) Clear sky OLR Jan/Feb, (d) Clear sky OLR Jun/Aug. Units are W/m²

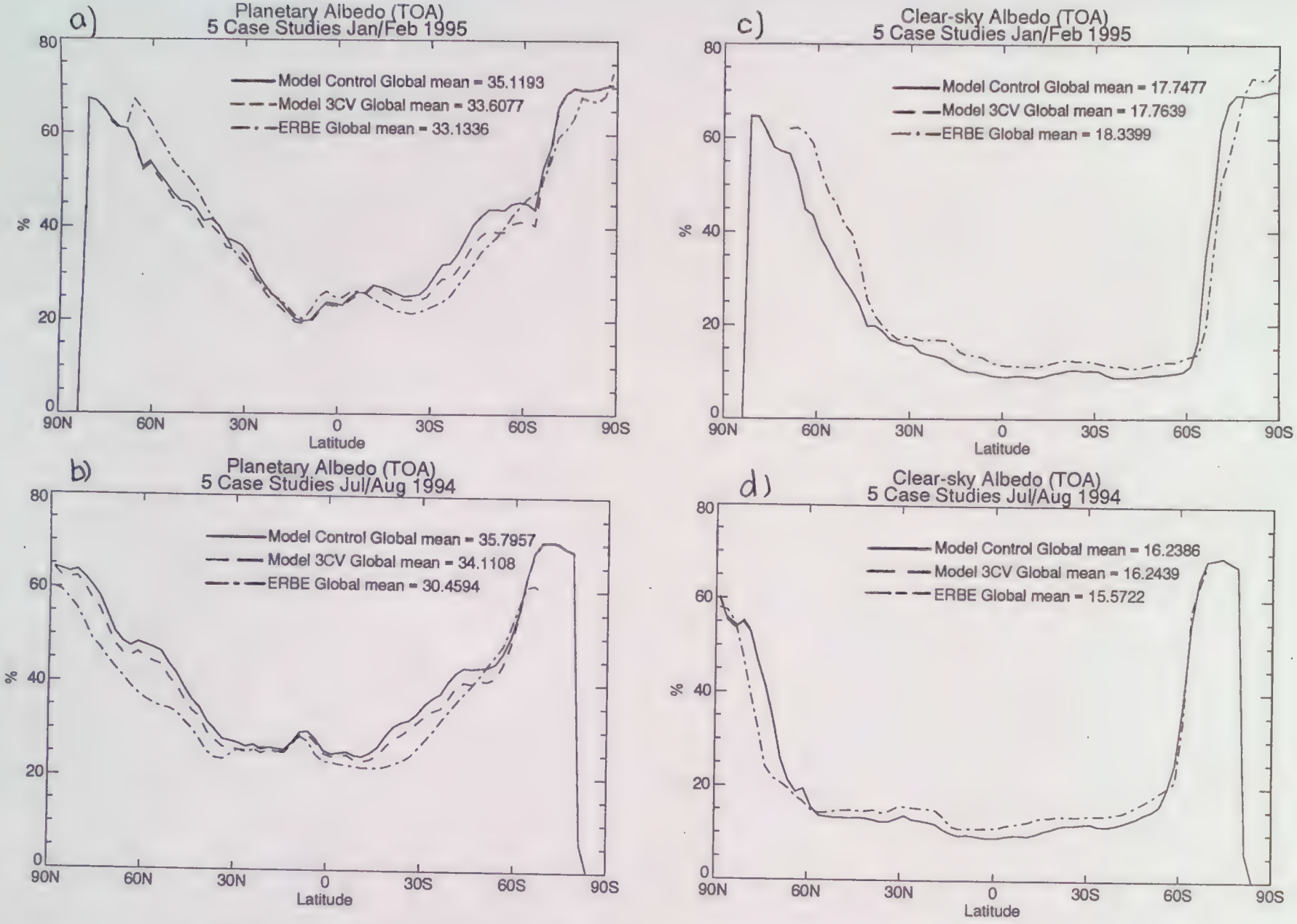

Figure 24 - Zonally averaged TOA radiative flux (T+96 to T+120) comparisons with ERBE data (1988), (a) albedo Jan/Feb, (b) albedo Jun/Aug, (c) Clear sky albedo Jan/Feb, (d) Clear sky albedo Jun/Aug. Units are W/m^2

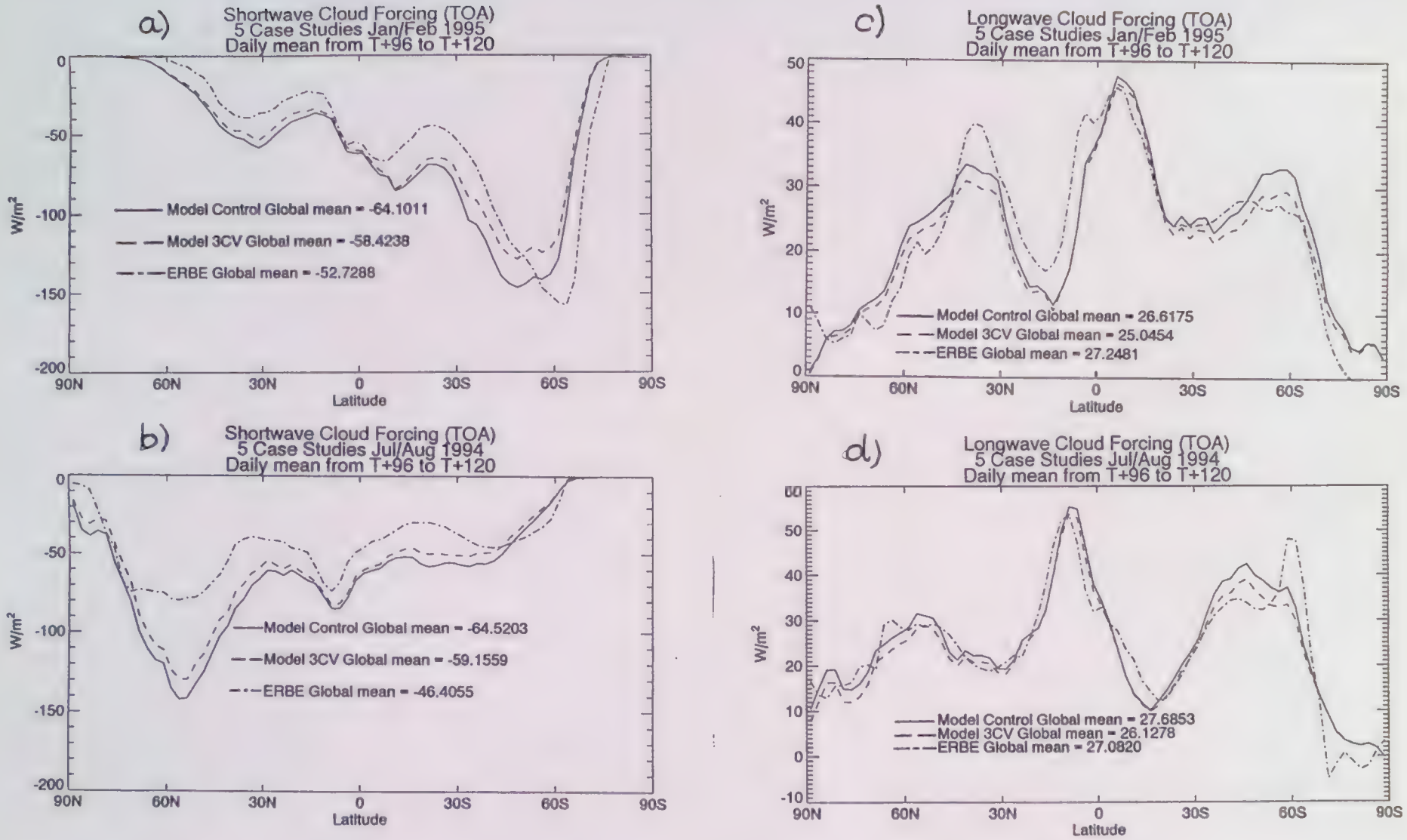

Figure 25 - Zonally averaged TOA radiative flux (T+96 to T+120) comparisons with ERBE data (1988), (a) SW cloud forcing Jan/Feb, (b) SW cloud forcing Jun/Aug, (c) LW cloud forcing Jan/Feb, (d) LW cloud for cing Jun/Aug. Units are W/m²

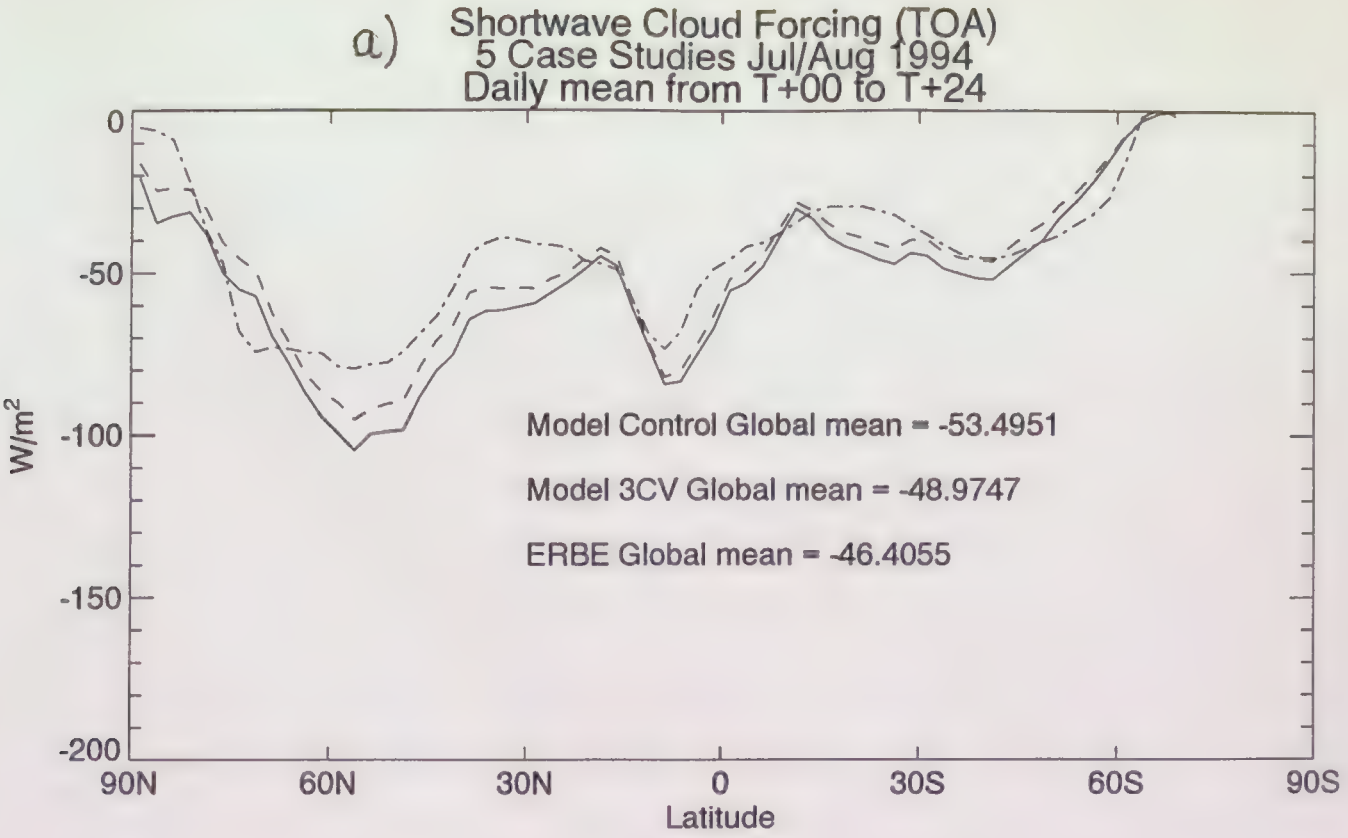

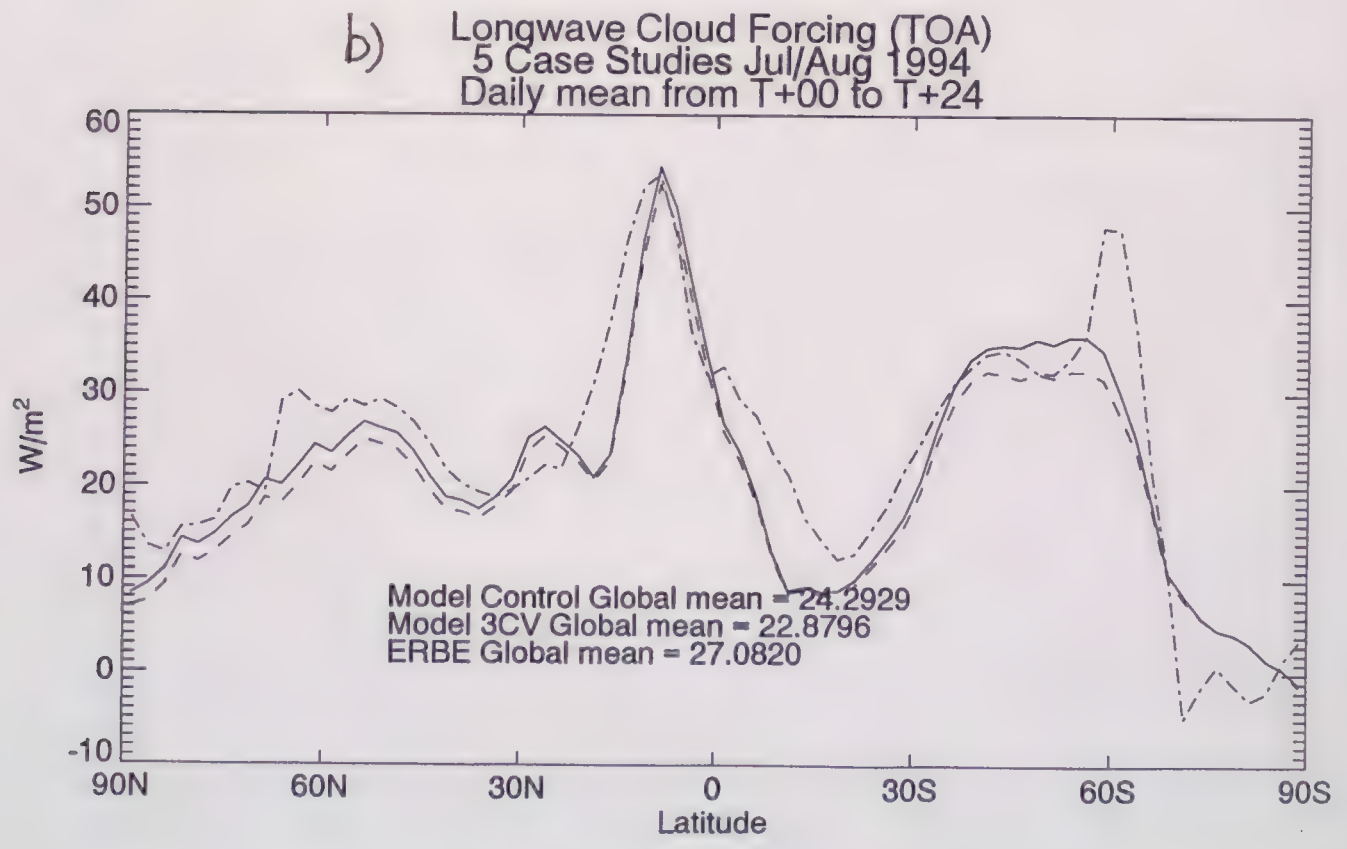

Figure 26 - Zonally averaged TOA radiative flux (T+00 to T+24) comparisons with ERBE data (1988), (a) SW cloud forcing Jun/Aug, (b) LW cloud forcing Jun/Aug. Units are W/m^2

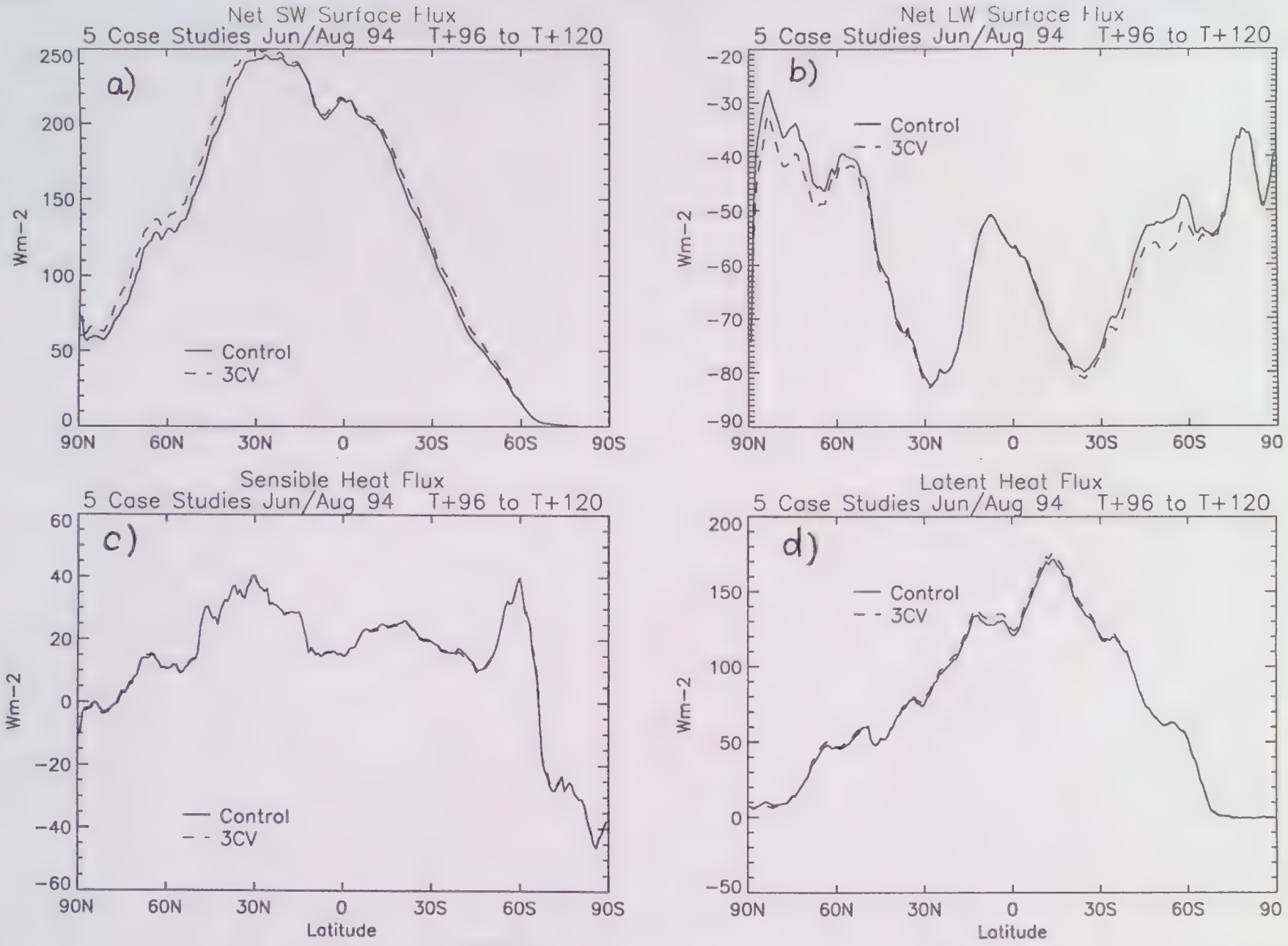

Figure 27 - Zonally averaged surface fluxes (T+96 to T+120) for Jun/Aug 94, (a) Net SW radiative flux, (b) net LW radiative flux (c) Sensible heat flux, (d) Latent heat flux. Units are W/m^2

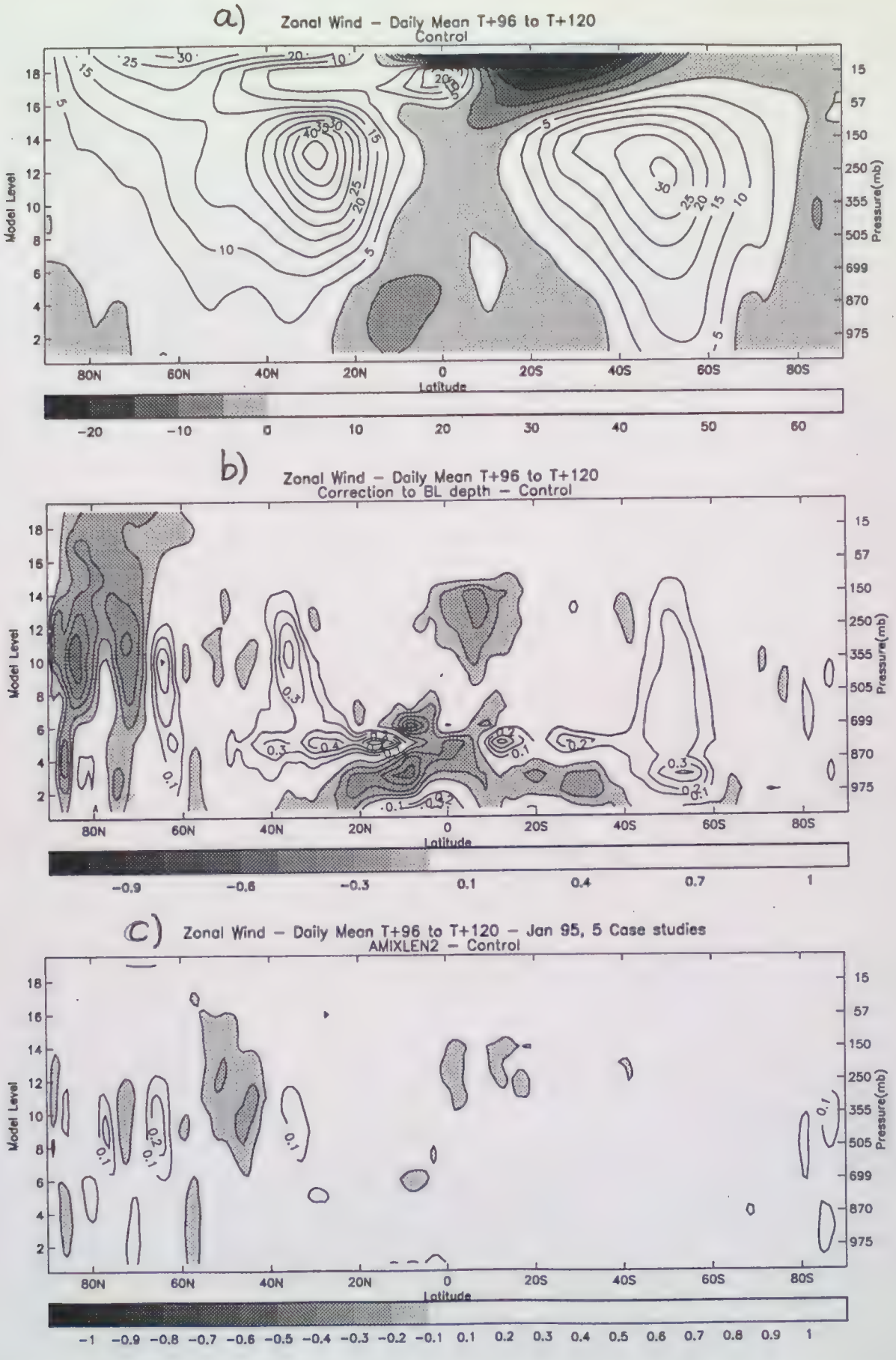

Figure 28 - Impact of experiments in BL turbulent mixing on the zonally averaged zonal wind at T+96 to T+120, (a) Control, (b) Correction to BL depth - Control, (c) ALENMIX2 (Correction to BL depth+double assymptotic mixing length) - Control

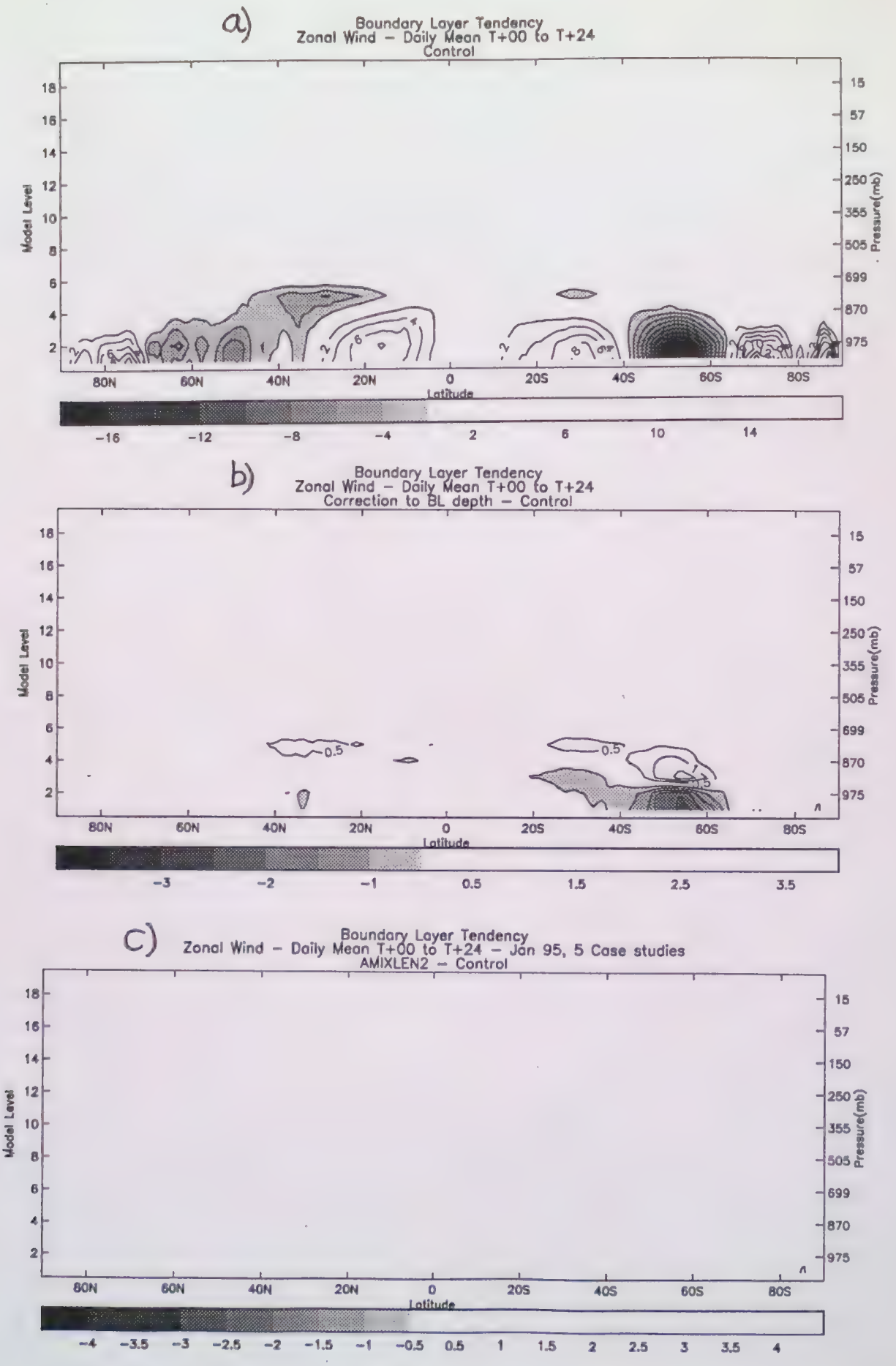

Figure 29 - as figure 28 but for BL zonal wind tendencies (m/s/day)

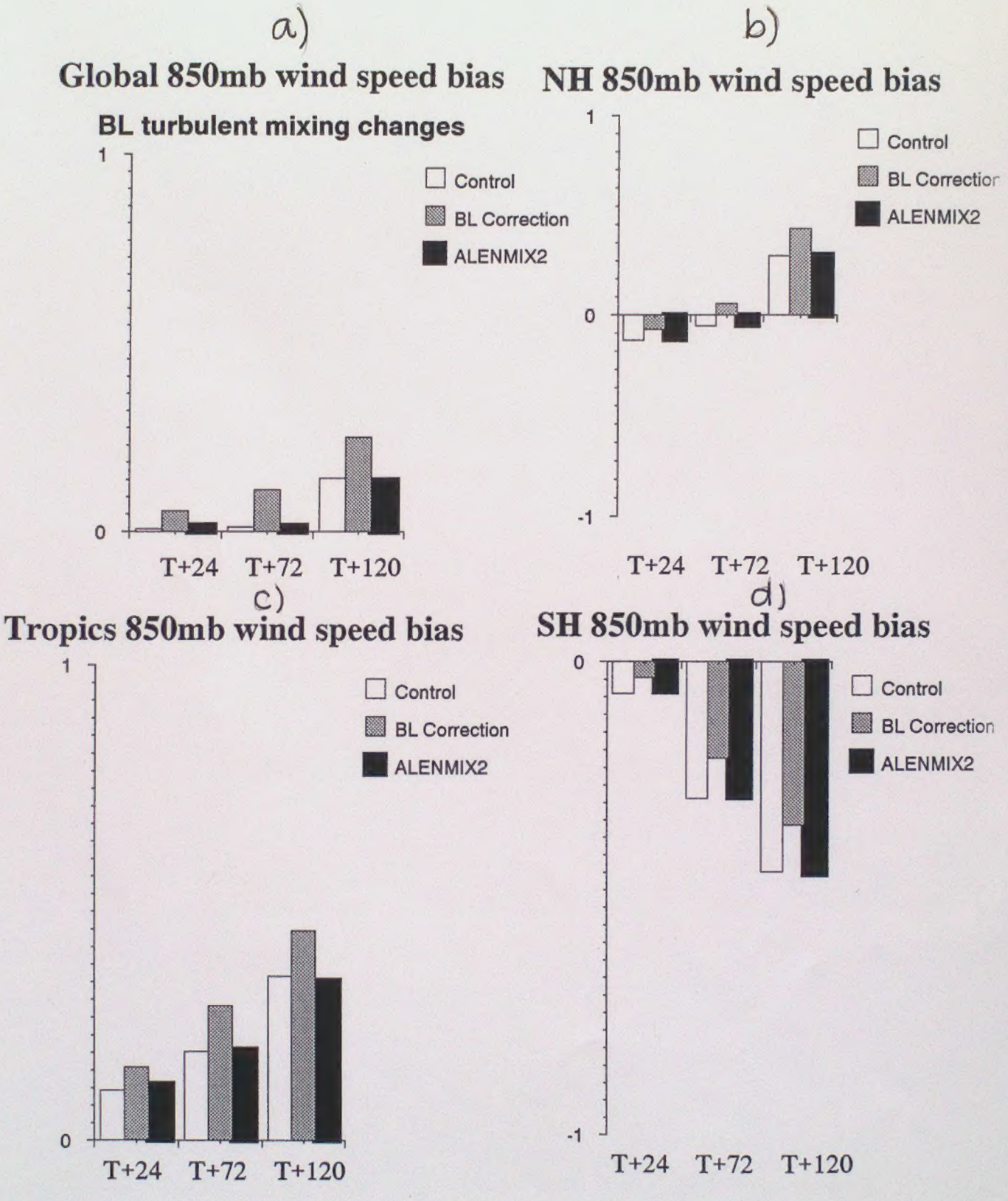

Figure 30 - Wind speed bias at 850mb for BL turbulent mixing experiments (a) Global, (b) Northern Hemisphere (90N-30N), (c) Tropics (30N-30S), (d) Southern Hemisphere (30S-90S).

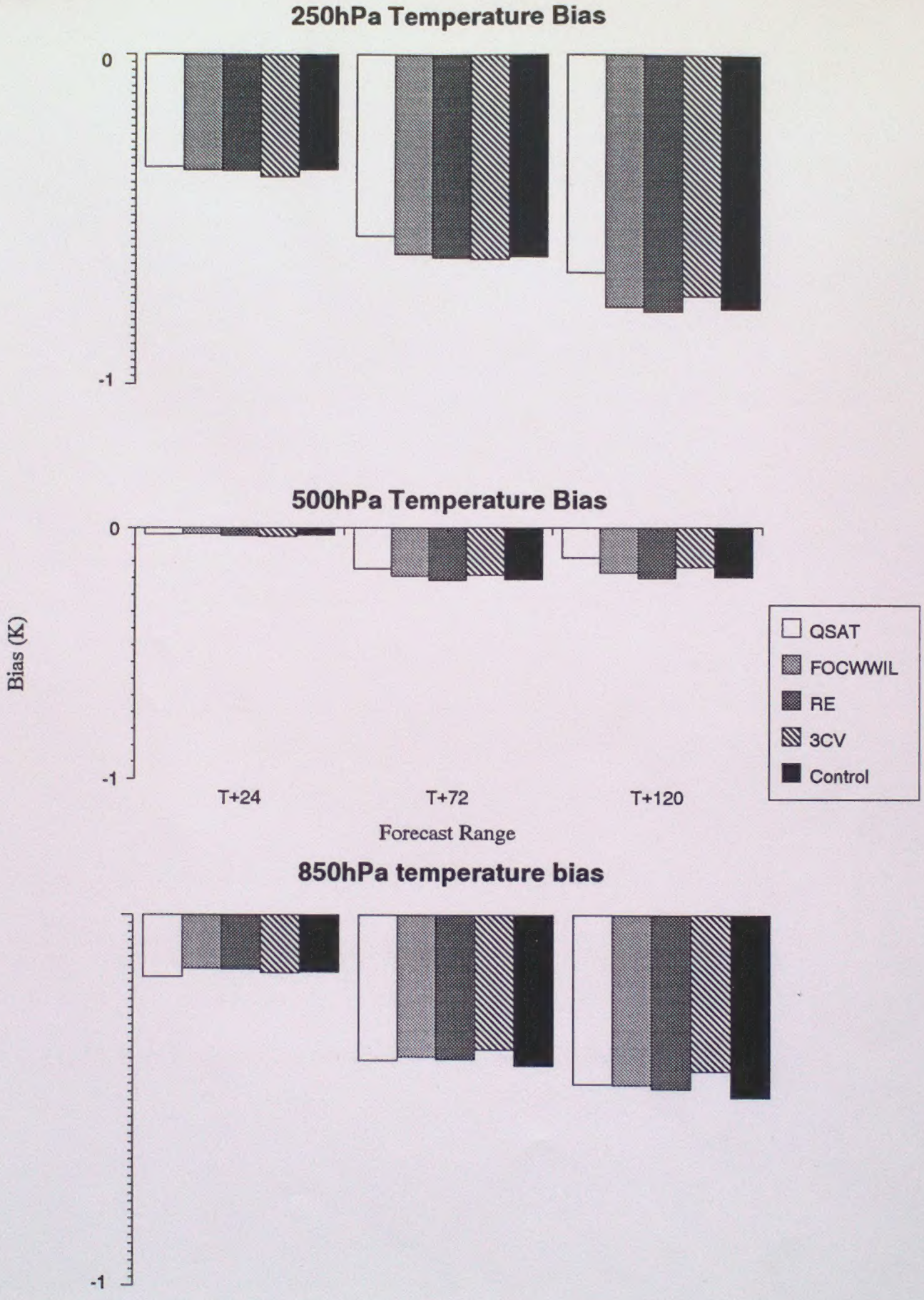

Figure 31 - Global temperature biases against analysis for the Jan/Feb 95 cases. Forecast ranges T+24, T+72 and T+120 are shown in each case. Temperature biases at 250hPa (upper panel), 500hPa (middle panel) and 850hPa (lower panel) are given.

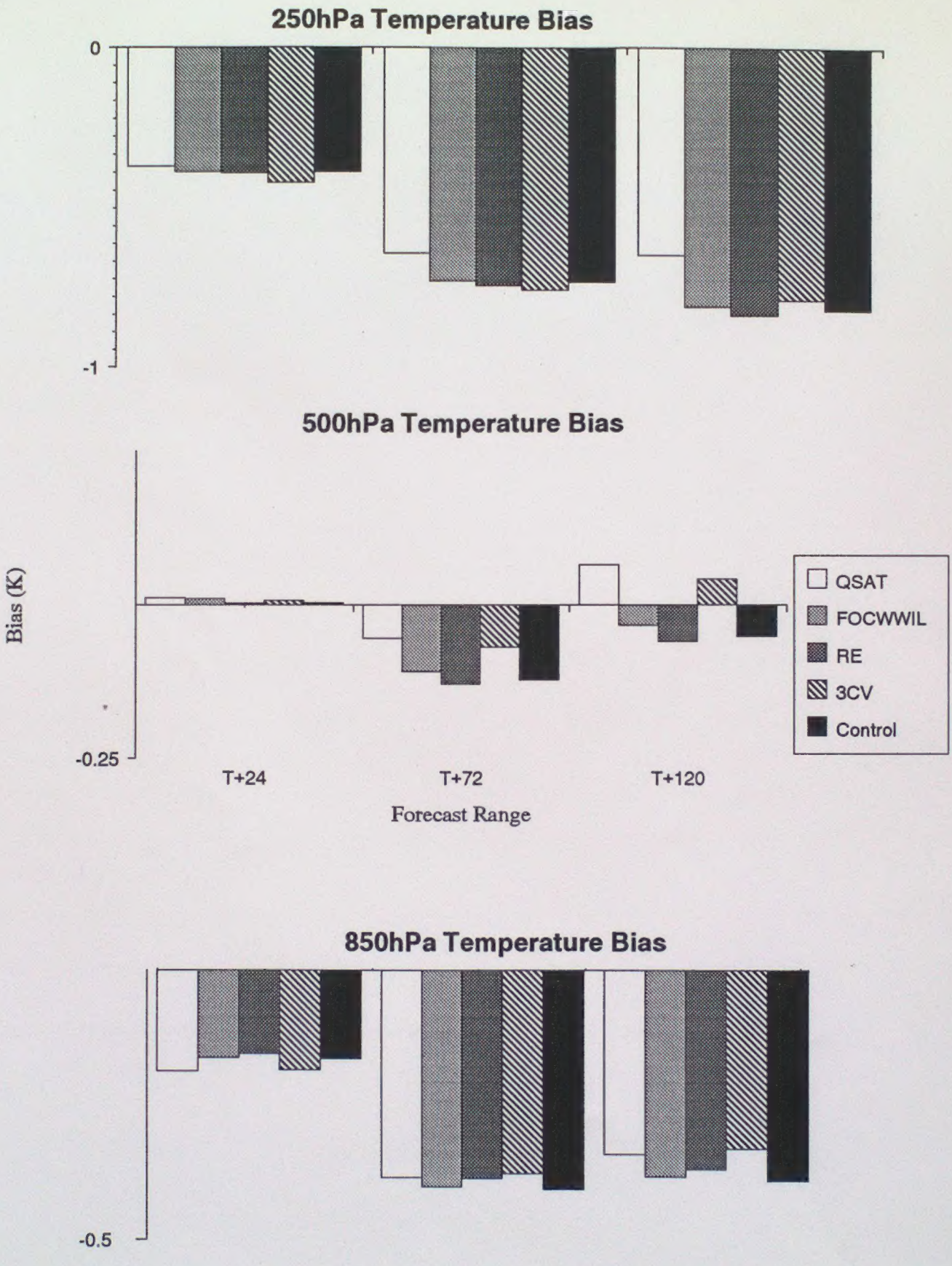

Figure 32 - As Figure 31, but for the tropics (30N-30S) only.

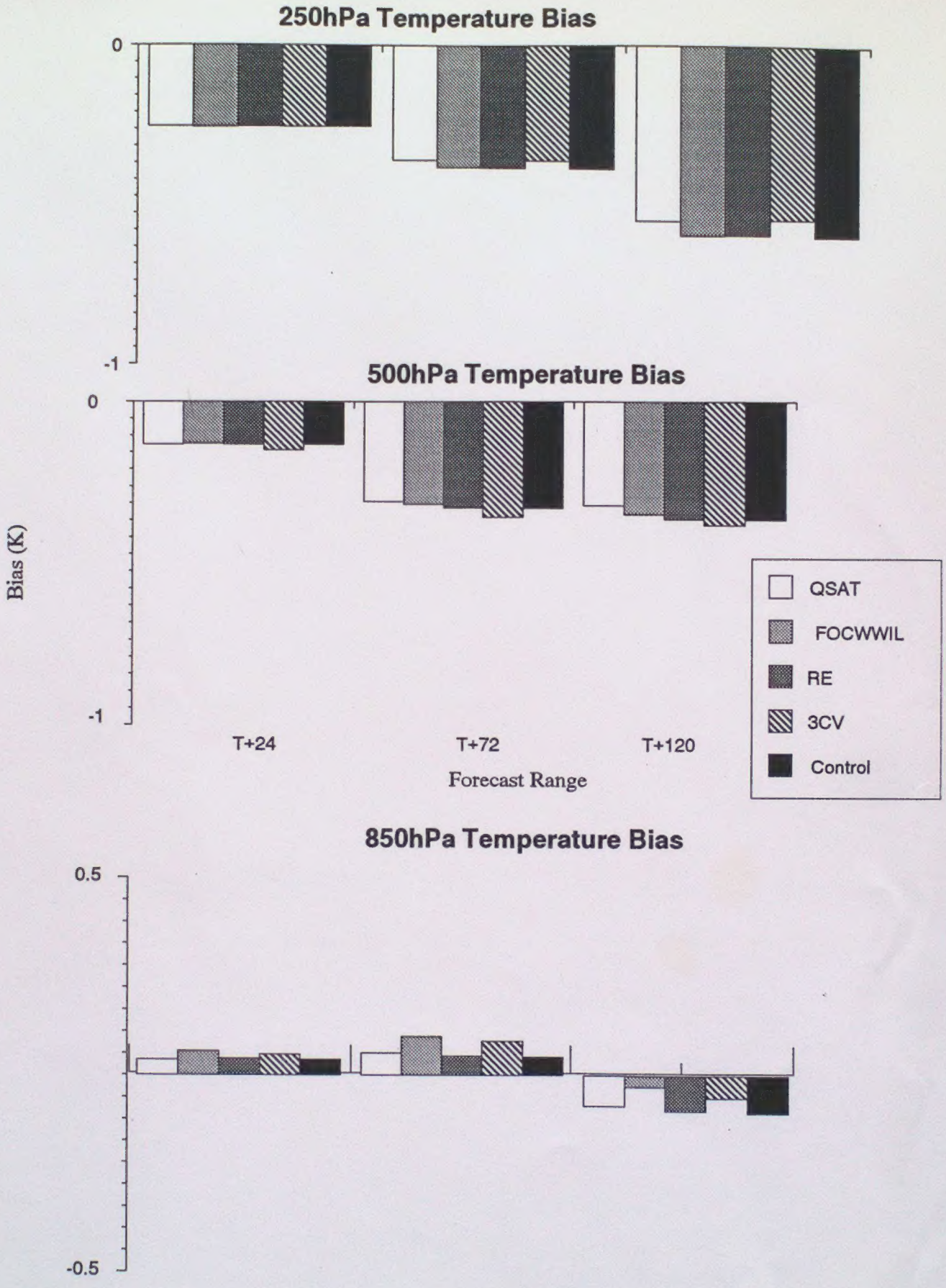

Figure 33 - As Figure 31, but for the northern hemisphere (30N-90N) only.